

THESIS FOR THE DEGREE OF DOCTOR OF PHILOSOPHY
IN
THERMO AND FLUID DYNAMICS

Development of Vortex Filament
Method for Wind Power
Aerodynamics

by

HAMIDREZA ABEDI

Department of Applied Mechanics
Division of Fluid Dynamics
CHALMERS UNIVERSITY OF TECHNOLOGY
Gothenburg, Sweden 2016

Development of Vortex Filament Method for Wind Power Aerodynamics
HAMIDREZA ABEDI
ISBN 978-91-7597-360-9

© HAMIDREZA ABEDI, 2016

Doktorsavhandlingar vid Chalmers tekniska högskola
Ny serie nr. 4041
ISSN 0346-718X

Department of Applied Mechanics
Division of Fluid Dynamics
Chalmers University of Technology
SE-412 96 Gothenburg
Sweden
Telephone: +46 (0)31-772 1000

Cover:
Free vortex wake modeling (subjected to turbulent inflow) for wind turbine aerodynamics.

This document was typeset using \LaTeX

Printed at Chalmers Reproservice
Gothenburg, Sweden 2016

Development of Vortex Filament Method for Wind Power Aerodynamics

HAMIDREZA ABEDI

Department of Applied Mechanics
Division of Fluid Dynamics
Chalmers University of Technology

ABSTRACT

Wind power is currently one of the cleanest and widely distributed renewable energy sources serving as an alternative to fossil fuel generated electricity. Exponential growth of wind turbines all around the world makes it apt for different research disciplines. The aerodynamics of a wind turbine is governed by the flow around the rotor, where the prediction of air loads on rotor blades in different operational conditions and its relation to rotor structural dynamics is crucial for design, development and optimization purposes. This leads us to focus on high-fidelity modeling of the rotor and wake aerodynamics. There are different methods for modeling the aerodynamics of a wind turbine with different levels of complexity and accuracy, such as the Blade Element Momentum (BEM) theory, Vortex method and Computational Fluid Dynamics (CFD). Historically, the vortex method has been widely used for aerodynamic analysis of airfoils and aircrafts. Generally, it may stand between the CFD and BEM methods in terms of the reliability, accuracy and computational efficiency. In the present work, a free vortex filament method for wind turbine aerodynamics was developed. Among different approaches for modeling the blade (e.g. a lifting line or a lifting surface) and wake (e.g. a prescribed or a free wake model), the Vortex Lattice Free Wake (VLFW) model known as the most accurate and computationally expensive vortex method was implemented. Because of the less restrictive assumptions, it could be used for unsteady load calculations, especially for time-varying flow environment which are classified according to the atmospheric conditions, e.g. wind shear and turbulent inflow together with the turbine structure such as yaw misalignment, rotor tilt and blade elastic deformation. In addition to the standard potential method for aerodynamic load calculation using the VLFW method, two additional methods, namely the 2D static airfoil data model and the dynamic stall model were implemented to increase capability of the free vortex wake method to predict viscous phenomena such as drag and separation using tabulated airfoil data. The implemented VLFW method was validated against the BEM and CFD methods, the GENUVP code by National Technical University of Athens (NTUA), Hönö turbine measurement data and MEXICO wind tunnel measurements. The results showed that the VLFW model might be used as a suitable engineering method for wind turbine's aerodynamics covering a broad range of operating conditions.

Keywords: Free wake model, vortex method, unsteady aerodynamic load, fatigue loads, wind turbine, forest canopy, large-eddy simulation, atmospheric turbulence

Although to penetrate into the intimate mysteries of nature and thence to learn the true causes of phenomena is not allowed to us, nevertheless it can happen that a certain fictive hypothesis may suffice for explaining many phenomena.

Leonhard Euler (15 April 1707–18 September 1783)

ACKNOWLEDGEMENTS

I would like to express my sincere gratitude to my supervisors, Professor Lars Davidson and Professor Spyros Voutsinas for their support, enlightening discussions, brilliant advices and encouragement. It was an unaccountable pleasure to work with them during these five years. "Thank you Lars and Spyros, words cannot describe how grateful you are".

I would like to thank Ingemar Carlen at Teknikgruppen AB for his valuable advices and insights. Special thanks go to Vasilis Riziotis and Petros Chasapogiannis for their supports during the study visits in National Technical University of Athens (NTUA).

I am grateful to my best friend, Alireza Majlesi for his endless and excellent contribution. I would like to thank my former colleagues, Mohammad Irannezhad for his valuable advices and Bastian Nebenführ for his contribution to provide atmospheric turbulence data.

Thanks to all my colleagues and friends at the division of Fluid Dynamics and SWPTC for creating a pleasant working atmosphere. Particularly, Ulla Lindberg-Thieme, Monica Vargman, Ola Carlson and Sara Fogelström for their grateful supports.

I would like to thank my previous and present office mates, Oskar Thulin and Johanna Matsfelt for making our shared office an enjoyable place where everything can be discussed.

My warmest and deepest sense of gratitude goes to my family; my father Abbas, the first teacher in my life, who taught me dignity and loyalty; my mother, Maryam, the teacher of love and kindness and my sister Fatemeh, for her companionship and patience. Abbas, Maryam and Fatemeh, "Thanks for your infinite love and support, I am so proud of you".

I would like to thank Dr. Gerard Schepers from Energy Research Centre of the Netherlands (ECN) to provide the measurement data of MEXICO wind turbine which have been supplied by the consortium carried out the EU FP5 project Mexico: 'Model rotor EXperiments In COntrolled conditions.

The technical support of National Technical University of Athens (NTUA) to use the GENUVP is gratefully acknowledged. (GENUVP is an unsteady flow solver based on vortex blob approximations developed for rotor systems by National Technical University of Athens).

This work was financed through the Swedish Wind Power Technology Centre (SWPTC). SWPTC is a research centre for the design and production of wind turbines. The purpose of the centre is to support Swedish industry with knowledge of design techniques and maintenance in the field of wind power. The work is carried out in six theme groups and is funded by the Swedish Energy Agency, by academic and industrial partners.

LIST OF PUBLICATIONS

This thesis consists of an extended summary and the following appended papers:

- Paper A** H. Abedi, L. Davidson, and S. Voutsinas. “Vortex method application for aerodynamic loads on rotor blades”. *EWEA 2013 Conference*. Vienna, Austria, 4–7 February, 2013
- Paper B** H. Abedi, L. Davidson, and S. Voutsinas. “Development of free vortex wake method for aerodynamic loads on rotor blades”. *EWEA 2014 Conference*. Barcelona, Spain, 10–13 March, 2014
- Paper C** H. Abedi, L. Davidson, and S. Voutsinas. “Development of free vortex wake method for yaw misalignment effect on the thrust vector and generated power”. *32nd AIAA Applied Aerodynamics Conference*. AIAA Aviation paper 2014-2847. Atlanta, GA, United States, 16–20 June, 2014
- Paper D** H. Abedi, L. Davidson, and S. Voutsinas. “Numerical studies of the upstream flow field around a horizontal axis wind turbine”. *33rd Wind Energy Symposium*. AIAA SciTech paper 2015-0495. Kissimmee, FL, United States, 5–9 January, 2015
- Paper E** H. Abedi, L. Davidson, and S. Voutsinas. “Development of free vortex wake model for wind turbine aerodynamics under yaw condition”. *34th Wind Energy Symposium*. AIAA SciTech paper 2016-1257. San Diego, CA, United States, 4–8 January, 2016
- Paper F** H. Abedi, L. Davidson, and S. Voutsinas. Enhancement of free vortex filament method for aerodynamic loads on rotor blades. *Submitted to Journal of Solar Energy Engineering* (2016)
- Paper G** H. Abedi, B. Nebenführ, L. Davidson, and S. Voutsinas. Assessment of the influence of turbulent inflow fields on wind-turbine power production. *to be submitted to a scientific journal* (2016)

DIVISION OF WORK

All papers were written by H. Abedi, who also developed the VLFW code and performed the numerical simulations including the prescribed wake models, free wake model and BEM method. All simulations with GENUVP code were done during H. Abedi's study visits at National Technical University of Athens (NTUA) with the help of Petros Chasapogiannis. In paper B, the CFD data provided by Denmark Technical University (DTU). In paper C, the experimental data of Hönö wind turbine were provided by Anders Wickström and Christian Haag from Scandinavian Wind AB. In paper D, E and G, the measurement data of MEXICO wind turbine were provided by Gerard Schepers from Energy Research Centre of the Netherlands (ECN) and have been supplied by the consortium which carried out the EU FP5 project Mexico: 'Model rotor EXperiments In COntrolled conditions'. In paper F, turbulent inflow fields generated by LES and synthetic turbulence (Mann model) were provided by Bastian Nebenführ. Lars Davidson and Spyros Voutsinas, the main supervisor and co-supervisor, respectively provided guidance and valuable discussion during the project.

CONTENTS

Abstract	i
Acknowledgements	v
List of publications	vii
Contents	ix
I Extended Summary	1
1 Introduction	1
2 Theory	5
2.1 Governing equation	5
2.2 Helmholtz's theorem	5
2.3 Potential flow	6
2.4 Correction methods for Biot-Savart's law	8
3 Application	13
3.1 Vortex Lattice Free Wake (VLFW)	14
3.1.1 Modeling	14
3.2 Load Calculation	20
3.2.1 The Standard Potential Method	20
3.2.2 2D Static Airfoil Data Method	22
3.2.3 Dynamic Stall Method	23
4 Summary of papers	25
4.1 Paper A	25
4.1.1 Summary	25
4.1.2 Comments	25
4.2 Paper B	26
4.2.1 Summary	26
4.2.2 Comments	26
4.3 Paper C	26
4.3.1 Summary	26
4.3.2 Comments	27
4.4 Paper D	28
4.4.1 Summary	28
4.4.2 Comments	28
4.5 Paper E	28
4.5.1 Summary	29
4.5.2 Comments	30

4.6 Paper F 30
4.6.1 Summary 30
4.6.2 Comments 31
4.7 Paper G 31
4.7.1 Summary 31
4.7.2 Comments 33

5 Concluding Remarks 35

References 37

A Extended ONERA Model 43

II Appended Papers A–G 47

Part I

Extended Summary

1 Introduction

The methods for predicting wind turbine performance are similar to propeller and helicopter theories. There are different methods for modeling the aerodynamics of a wind turbine with different levels of complexity and accuracy, such as the BEM theory and solving the Navier-Stokes equations using Computational Fluid Dynamics (CFD).

Today, an engineering model based on the Blade Element Momentum (BEM) method is extensively used for analyzing the aerodynamic performance of a wind turbine where it is based on the steady and homogeneous flow assumption and aerodynamic loads act on an actuator disc instead of a finite number of blades. The BEM method is known as the improved model of the Rankine-Froude momentum theory [8, 9], which was the first model to predict inflow velocities at the rotor, where it assumes that the rotor can be replaced by a uniformly loaded actuator disc, and the inflow is uniform as well. Moreover, Prandtl's hypothesis is the foundation of the BEM method, assuming that a section of a finite wing behaves as a section of an infinite wing at an angle equal to the effective angle of attack. The BEM method is computationally fast and is easily implemented, but it is acceptable only for a certain range of flow conditions [10, 11]. A number of empirical and semi-empirical correction factors have been added to the BEM method in order to increase its application range, such as yaw misalignment, dynamic inflow, dynamic stall, tower influence, finite number of blades and blade cone angle [12], but they are not relevant to all operating conditions and are often incorrect at high tip speed ratios where wake distortion is significant [13]. The existence of the number of correction formula leads to uncertainties to the BEM method, while the foundation of such corrections is based on experimental results, decreasing the reliability of the BEM method.

The vortex theory, which is based on the inviscid, incompressible and irrotational flow (potential flow), can also be used to predict the aerodynamic performance of wind turbines. It has been widely used for aerodynamic analysis of airfoils and aircrafts. Although the standard method cannot be used to predict viscous phenomena such as drag and boundary layer separation, its combination with tabulated airfoil data makes it a powerful tool for prediction of fluid flow. Compared with the BEM method, the vortex method is able to provide more physical solutions for attached flow conditions using boundary layer corrections, and it is also valid over a wider range of turbine operating conditions. Although it is computationally more expensive than the BEM method, it is still feasible as an engineering method.

The early vortex method application was introduced by Glauert [14, 15], Prandtl [16] and Goldstein [17]. In Glauert's theory, instead of a finite number of blades, the rotor is modeled as a uniformly loaded actuator disc and the wake is modeled as a semi-infinite cylindrical sheet of vortices that is shed from the edge of an actuator disk. Prandtl's method introduced radial inflow distribution, which leads to the tip-loss factor concept

correcting the assumption of an infinite number of blades. Goldstein’s theory represents the inflow by assuming the trailing vortices of each blade as a finite number of infinite length coaxial helicoidal surfaces but with a finite radius moving at a constant velocity. Falkner [18] used the vortex lattice method in 1943 to calculate aerodynamic forces on a surface of arbitrary shape. This method is still used in engineering applications because it requires relatively small computational time with a level of accuracy compared with CFD. Reviews of historical development of rotor aerodynamics have recently been published by Okulov, Sørensen and van Kuik [19–23].

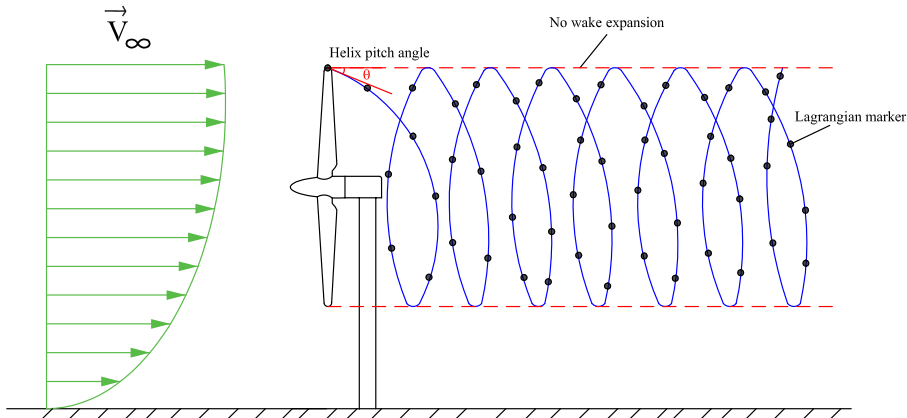


Figure 1.1: *Schematic of prescribed vortex wake model*

In vortex methods, the trailing and shed vortices are modeled by either vortex particles [24–26] or vortex filaments [27, 28] moving either freely, known as free wake [29–31] or restrictedly by imposing the wake geometry, known as prescribed wake [32, 33]. The prescribed wake requires less computational effort than the free wake, but it requires experimental data to be valid for a broad range of operating conditions. The free wake model, which is the most computationally expensive vortex method, is able to predict the wake geometry and loads more accurately than the prescribed wake because of less restrictive assumptions. Therefore, it can be used for load calculations, especially for unsteady flow environment which are classified according to the atmospheric conditions, e.g. wind shear and turbulent inflow together with the turbine structure such as yaw misalignment, rotor tilt and blade elastic deformation [34]. However, its application is limited to attached flow and it must be linked to tabulated airfoil data to predict the air loads in the presence of the drag and the flow separation.

The vortex method has historically been used for helicopters [35–37] to model the wake and aerodynamic loads for different operational conditions. Landgrebe [38] developed a prescribed wake consisting of a number of filaments shed into the wake from the blade trailing edge that are rolled up immediately into a tip vortex. An analytical approach to predict propellers’ inflow by using lifting line theory, was described by Crimi [39], where the wake is replaced by a single tip vortex and moved based on the induced velocity field during the blade rotation. Several simplified methods by Brady [40] and Trenka [41]

have been developed to model the wake by vortex rings or vortex tubes. Landgrebe [38], Leishman [42] and Sadler [43] also proposed a free wake model for helicopters, where the wake is modeled by segmented vortex filaments which are allowed to distort freely. For wind turbine applications, Coton [44], Dumitrescu [45], Kocurek [46] and Curin [47] introduced the prescribed vortex filament wake model in addition to a work by Gohard [48], which is regarded as a pioneer free wake model for wind turbines.

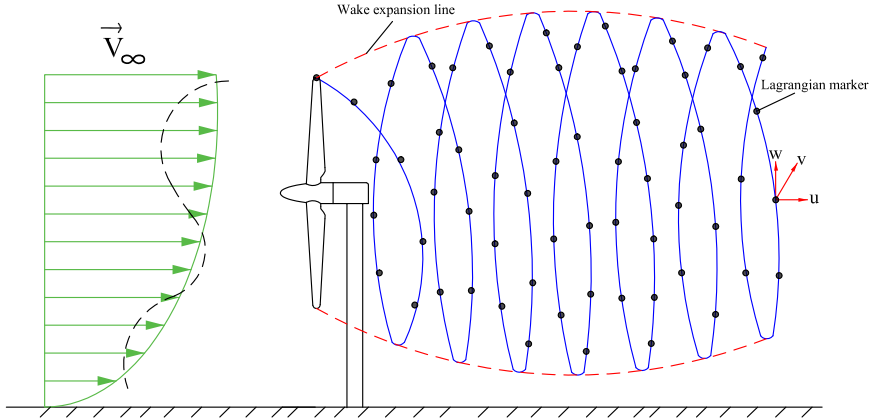


Figure 1.2: *Schematic of free vortex wake model*

Finally, CFD, which solves the Navier-Stokes equations for the flow around the rotor blade [49–54], is known as the most accurate but computationally most expensive method making it an impractical engineering method for wind turbine applications, at least with the current computational hardware resources.

To overcome this limitation, a combination of Navier-Stokes equations and an actuator disc method was proposed by Madsen [55], where instead of resolving the viscous flow around the rotor blades, the swept surface of the rotor blade is replaced by surface forces acting upon the inflow. Another method called actuator line was proposed by Sørensen [49] where the air load is distributed radially in the solution domain along the lines representing the blade forces. In this method, the blade element method and airfoil data are used to determine the aerodynamic loads while the wake is simulated by a 3D Navier-Stokes solver. The hybrid CFD-Inviscid method was proposed by Berkman [56], Xu [57] and Schmitz [58] in order to remove the dependency on the tabulated airfoil data while a small region around the blade is solved by Navier-Stokes equations and a full potential vortex method is applied for the rest of the computational domain.

2 Theory

2.1 Governing equation

The governing equation of an incompressible, inviscid fluid is given by Euler's equations expressing the conservation of mass and momentum as

$$\begin{aligned}\nabla \cdot \mathbf{v} &= 0 \\ \frac{\partial \mathbf{v}}{\partial t} + \mathbf{v} \cdot \nabla \mathbf{v} &= -\frac{\nabla p}{\rho}\end{aligned}\tag{2.1}$$

where \mathbf{v} , t , p and ρ denote the velocity, time, pressure and density, respectively. Recall the vorticity field is defined as the curl of a velocity field $\boldsymbol{\Omega} = \nabla \times \mathbf{v}$, and for a constant-density flow the curl of the inviscid momentum equation gives the inviscid vorticity transport equation as

$$\begin{aligned}\frac{\partial \boldsymbol{\Omega}}{\partial t} + \mathbf{v} \cdot \nabla \boldsymbol{\Omega} &= (\boldsymbol{\Omega} \cdot \nabla) \mathbf{v} \\ \frac{D \boldsymbol{\Omega}}{Dt} &= (\boldsymbol{\Omega} \cdot \nabla) \mathbf{v}\end{aligned}\tag{2.2}$$

where the right-hand side term denotes the tilting and stretching of vorticity (in an inviscid fluid the vortex lines/tubes move with the fluid according to the Helmholtz theorem).

A region containing a concentrated amount of vorticity is called a vortex, where a vortex line is defined as a line whose tangent is parallel to the local vorticity vector everywhere. Vortex lines surrounded by a given closed curve form a vortex tube. A vortex tube of an infinitesimal cross-section, immersed in irrotational fluid, is called vortex filament [59]. In rotor aerodynamics modeling, the vortical structure of a wake may be modeled by either vortex filaments or vortex particles. In the vortex filament approach, each vortex wake element is generally introduced as a straight line segment [60–66] containing two points, one at the head and another at the tail, which are known as Lagrangian markers. A vortex filament may also be presented as a curvilinear segment by fitting a parabolic arc through three adjacent marker points [64, 67–69].

2.2 Helmholtz's theorem

The dynamics of fluid elements carrying vorticity was proposed by Helmholtz for inviscid transport of vorticity. According to Helmholtz's theorem, the strength of a vortex tube is constant along its length and does not vary with time. In addition, an irrotational motion of an inviscid fluid started from rest remains irrotational. Lastly, a vortex line cannot end in the fluid; it must form a closed path, end at a solid boundary or go to infinity, implying that vorticity can only be generated at solid boundaries. Therefore, a solid surface may be considered as a source of vorticity. This leads to replace the solid surface in contact with fluid by a distribution of vorticity.

The extension of Helmholtz's theorem to take the viscosity effects into account [70] is called Kelvin's theorem given by

$$\frac{D\Gamma}{Dt} = \oint_c \frac{D\mathbf{v}}{Dt} \cdot d\mathbf{l} \quad (2.3)$$

where by replacing \mathbf{v} with Navier-Stokes' equations, it may be written as

$$\frac{D\Gamma}{Dt} = - \oint_c \frac{\nabla p}{\rho} \cdot d\mathbf{l} + \oint_c \nu \nabla^2 \mathbf{v} \cdot d\mathbf{l} \quad (2.4)$$

where Γ and ν denote the circulation and kinematic viscosity, respectively. For an inviscid and incompressible flow, Eq. (2.4) reduces to

$$\frac{D\Gamma}{Dt} = 0 \quad (2.5)$$

where it implies that in the absence of density variations and viscosity, the circulation is conserved; it is constant around any closed curve moving with the fluid. This is another proof of Helmholtz's theorem which states that an irrotational motion of an inviscid fluid started from rest remains irrotational.

2.3 Potential flow

An inviscid ($\nu = 0$), incompressible ($\nabla \cdot \mathbf{v} = 0$) and irrotational ($\nabla \times \mathbf{v} = 0$) flow is called potential flow governed by Laplace's equation as

$$\begin{aligned} \nabla \cdot \mathbf{v} &= 0 \\ \mathbf{v} &= \nabla \Phi \\ \nabla^2 \Phi &= 0 \end{aligned} \quad (2.6)$$

where Φ denotes the velocity potential. Solving Laplace's equation with a proper boundary condition yields the velocity field (\mathbf{v}) based on the velocity potential (Φ) where consequently the pressure field may be determined using Bernoulli's equation.

For a finite area of fluid, a quantity corresponding to vorticity is the circulation. In other words, circulation is the amount of fluid vorticity in an open surface enclosed by the curve where it is mathematically expressed (using Stokes' theorem) as

$$\Gamma = \oint_c \mathbf{v} \cdot d\mathbf{l} = \int_A (\nabla \times \mathbf{v}) \cdot \mathbf{n} dA = \int_A \boldsymbol{\Omega} \cdot \mathbf{n} dA \quad (2.7)$$

An illustration may be a vortex flow which is based on the incompressible ($\nabla \cdot \mathbf{v} = 0$) and irrotational ($\nabla \times \mathbf{v} = 0$) flow [71] at every point except at the origin of the vortex (infinite velocity). For a vortex flow (see Fig. 2.1), the tangential and radial velocity components are then given by

$$\begin{aligned} v_\theta &= \frac{C}{r} \\ v_r &= 0 \end{aligned} \quad (2.8)$$

where C is obtained by taking the circulation (see Eq. (2.7)) around a given circular streamline of radius r as

$$\Gamma = \oint_c \mathbf{v} \cdot d\mathbf{l} = v_\theta(2\pi r) \quad (2.9)$$

$$v_\theta = \frac{\Gamma}{2\pi r}$$

By comparing Eqs. (2.8) and (2.9), we get

$$C = \frac{\Gamma}{2\pi} \quad (2.10)$$

where Γ is termed the strength of the vortex flow. Equation (2.9) gives the velocity field for a vortex flow of strength Γ and the circulation taken around all streamlines is the same value, i.e. $\Gamma = 2\pi C$.

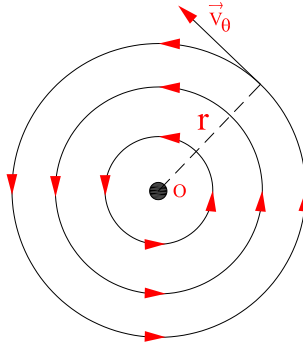


Figure 2.1: *Vortex flow*

According to vector analysis of fluid dynamics [13, 72, 73], any velocity field can be decomposed into a solenoidal field (divergence-free) and an irrotational field (curl-free) the so-called Helmholtz's decomposition as

$$\mathbf{v} = \mathbf{v}_\omega + \mathbf{v}_p \quad (2.11)$$

$$\mathbf{v} = \nabla \times \mathbf{\Psi} + \nabla\Phi$$

where $\mathbf{\Psi}$ is a vector potential and Φ is a scalar potential. By definition, \mathbf{v}_ω is the velocity field due to the vorticity in the flow and \mathbf{v}_p is the irrotational velocity field required to satisfy boundary condition in the presence of solid boundaries (zero-normal boundary condition). Taking the curl of Eq. (2.11) yields

$$\nabla \times \mathbf{v} = \nabla \times (\nabla \times \mathbf{\Psi}) + \nabla \times \nabla\Phi = \nabla \times (\nabla \times \mathbf{\Psi}) \quad (2.12)$$

According to vector identity

$$\nabla^2 \mathbf{\Psi} = \nabla (\nabla \cdot \mathbf{\Psi}) - \nabla \times (\nabla \times \mathbf{\Psi}) \quad (2.13)$$

$$\nabla^2 \mathbf{\Psi} = -\nabla \times (\nabla \times \mathbf{\Psi})$$

where $\nabla(\nabla \cdot \boldsymbol{\Psi}) = 0$ since $\boldsymbol{\Psi}$ is a divergence-free solenoidal vector field (also known as a vector stream function). From Eqs. (2.12), (2.13) and the definition of the vorticity field ($\nabla \times \mathbf{v} = \boldsymbol{\Omega}$), Poisson's equation for the vector potential is derived as

$$\nabla^2 \boldsymbol{\Psi} = -\boldsymbol{\Omega} \quad (2.14)$$

The solution of Poisson's equation expressed by Green's formula is

$$\boldsymbol{\Psi}(\mathbf{x}) = \frac{1}{4\pi} \int_V \frac{\boldsymbol{\Omega}(\mathbf{x}')}{|\mathbf{x} - \mathbf{x}'|} d\mathbf{x}' \quad (2.15)$$

where \mathbf{x} and \mathbf{x}' denote the position of point where the potential is computed and the position of the volume element $d\mathbf{x}'$, respectively. Generally, a prime denotes evaluation at the point of integration \mathbf{x}' , which is taken over the region where the vorticity is non-zero (the region occupied by fluid), designated by $d\mathbf{x}'$. According to Helmholtz's decomposition (see Eq. (2.11)), any velocity field can be presented as the summation of a rotational component which is induced by the vorticity field in an infinite space and a potential component which is required to satisfy the boundary condition [72, 73]. Therefore, the induced velocity (rotational component) field is obtained by taking the curl of Eq. (2.15) as

$$\mathbf{v}_{ind}(\mathbf{x}) = -\frac{1}{4\pi} \int_V \frac{(\mathbf{x} - \mathbf{x}') \times \boldsymbol{\Omega}}{|\mathbf{x} - \mathbf{x}'|^3} d\mathbf{x}' \quad (2.16)$$

which represents the well-known Biot-Savart's law. For a straight vortex filament of finite length with the strength of Γ , the Biot-Savart law [74–77] is written as

$$\mathbf{v}_{ind} = \frac{\Gamma}{4\pi} \frac{d\mathbf{l} \times \mathbf{r}}{|\mathbf{r}|^3} \quad (2.17)$$

It can also be expressed as

$$\mathbf{v}_{ind} = \frac{\Gamma}{4\pi} \frac{(r_1 + r_2)(\mathbf{r}_1 \times \mathbf{r}_2)}{(r_1 r_2)(r_1 r_2 + \mathbf{r}_1 \cdot \mathbf{r}_2)} \quad (2.18)$$

where \mathbf{r}_1 , \mathbf{r}_2 are the distance vectors from the beginning, A , and end, B , of a vortex segment to an arbitrary point C , respectively (see Fig. 2.2).

2.4 Correction methods for Biot-Savart's law

Biot-Savart's law has a singularity when the point of evaluation for induced velocity is located on the vortex filament axis. Likewise, when the evaluation point is very near to the vortex filament, there is an unphysically large induced velocity at that point. The remedy is either to use a cut-off radius, δ [78], or to use a viscous vortex model with a finite core size by multiplying a factor to remove the singularity [42]. Apart from an analytical solution of Biot-Savart's law, a numerical integration over the actual filament geometry, including smoothing methods to remove the singular part of Biot-Savart's law, may also be done to compute the velocity induced by a vortex filament [59, 67, 69, 70, 79–82].

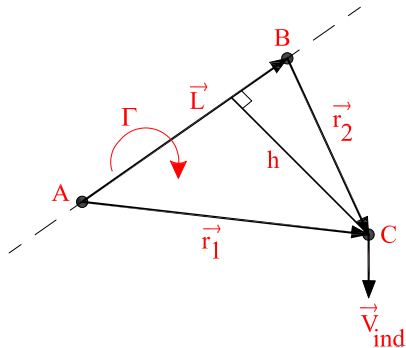


Figure 2.2: *Schematic for Biot-Savart's law*

Correction of Biot-Savart's law on the basis of the viscous vortex model can be done by introducing a finite core size, r_c , for a vortex filament [59, 75, 83–86]. Since the induced velocity field has a significant effect on the wake geometry and rotor aerodynamic loads, a suitable viscous core model thus increases the accuracy of the entire flow field.

There are two general approaches representing the viscous vortex model. The first is proposed based on the desingularized algebraic profile, i.e., a constant viscous core model such as Rankine [87], Scully [79, 88] and Vassitas [89] models. The second approach is a diffusive viscous core model where the vortex core size grows with time according to Lamb-Oseen's model [84]. In the present work, a constant viscous core model, which is used extensively in engineering applications, is employed for the correction of Biot-Savart's law.

For rotorcraft applications, Bagai [90] suggested the velocity profile based on Vassitas' model (see Eq. (2.19)) for $n = 2$. Vassitas' model is based on a general form of a desingularized algebraic swirl-velocity profile for stationary vortices expressed as

$$v_{\theta}(r) = \frac{\Gamma}{2\pi r} \left(\frac{r^2}{(r_c^{2n} + r^{2n})^{1/n}} \right) \quad (2.19)$$

where r , r_c and n is the distance from a vortex segment to an arbitrary point, the viscous core radius and an integer number, respectively. For $n = 1$ and $n \rightarrow \infty$, Eq. (2.19) resembles Scully's model and Rankine's model, respectively.

In order to take the effect of viscous vortex core into account, a factor of K_v must be added to the velocity induced by a straight vortex filament of finite length given by Biot-Savart's law as

$$\mathbf{v}_{ind} = K_v \frac{\Gamma}{4\pi} \frac{(r_1 + r_2)(\mathbf{r}_1 \times \mathbf{r}_2)}{(r_1 r_2)(r_1 r_2 + \mathbf{r}_1 \cdot \mathbf{r}_2)} \quad (2.20)$$

where

$$K_v = \frac{h^2}{(r_c^{2n} + h^{2n})^{1/n}} \quad (2.21)$$

and h is defined as the perpendicular distance of the evaluation point as (see Fig. 2.2)

$$h = \frac{|\mathbf{r}_1 \times \mathbf{r}_2|}{|\mathbf{L}|} \quad (2.22)$$

Factor K_v desingularizes Biot-Savart's equation when the evaluation point distance tends to zero and prevents a high induced velocity in the vicinity region of the vortex core radius. Figure 2.3 shows the effect of vortex viscous core model on the swirl (tangential) velocity.

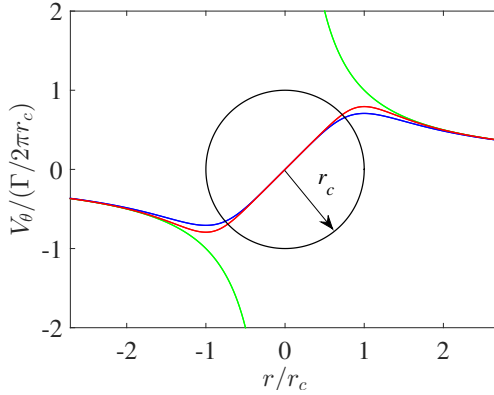


Figure 2.3: *Tangential velocity induced by a straight infinite vortex filament using different viscous core correction models, —: ideal vortex, —: Vassitas' model ($n = 2$), —: Vassitas' model ($n = 3$), —: Vortex core*

Generally, the distance parameter in correction factor (K_v) of Biot-Savart's law proposed by different models [42, 59, 73, 79, 83, 84, 89, 91], is the perpendicular distance (h) from the vortex filament segment to any arbitrary evaluation point. In other words, the classical correction factor K_v does only take into account the perpendicular distance between the vortex filament segment and the evaluation point regardless the geometrical configuration between the evaluation point and vortex filament.

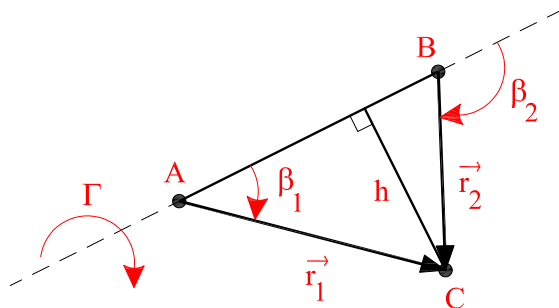


Figure 2.4: *Schematic for correction of Biot-Savart's law*

Van Hoydonck [67] showed that the classical correction factor K_v fails if the projection of the evaluation point falls beyond the beginning and end of a vortex segment. He proposed an improved correction factor K_v with respect to the beginning and end of a vortex segment (see Fig. 2.4) where it is given by

$$K_v = \frac{d^2}{(r_c^{2n} + d^{2n})^{1/n}} \quad \text{where} \quad \begin{cases} d = r_1, & \text{if } \cos \beta_1 < 0; \\ d = r_2, & \text{if } \cos \beta_2 > 0; \\ d = h, & \text{otherwise.} \end{cases} \quad (2.23)$$

where

$$\begin{aligned} \mathbf{r}_0 &= \mathbf{r}_1 - \mathbf{r}_2 \\ \cos \beta_1 &= \frac{\mathbf{r}_1 \mathbf{r}_0}{r_1 r_0} \\ \cos \beta_2 &= \frac{\mathbf{r}_2 \mathbf{r}_0}{r_2 r_0} \end{aligned} \quad (2.24)$$

In the early stage of present work, following Bagai's suggestion [90], a factor of K_v was employed to desingularize Biot-Savart's law. But later, K_v was defined according to Eq. (2.23) proposed by Van Hoydonck [67].

3 Application

The rotor inflow distribution is a key parameter in studies of aerodynamic loads on rotor blades and is highly dependent on the wake geometry. Hence, predicting the geometry of trailing wake vortices and their strength makes it possible to analyze wind turbine aerodynamic performance. In other words, suitable modeling of the blade and trailing wake has a great influence on the prediction of air load at the rotor blade.

Modeling the blade and wake by vortex filament method may be done by different approaches. In these methods which are constructed on the basis of some assumptions, the blade is modeled by either lifting line (originally proposed by Prandtl in 1921) or lifting surface, and the wake is modeled by either trailing horseshoe vortices or vortex ring elements. This results in different rotor aerodynamic modeling such as lifting line prescribed wake, lifting line free wake, vortex lattice prescribed wake and vortex lattice free wake. In the prescribed wake model, the wake that is shed from the blade trailing

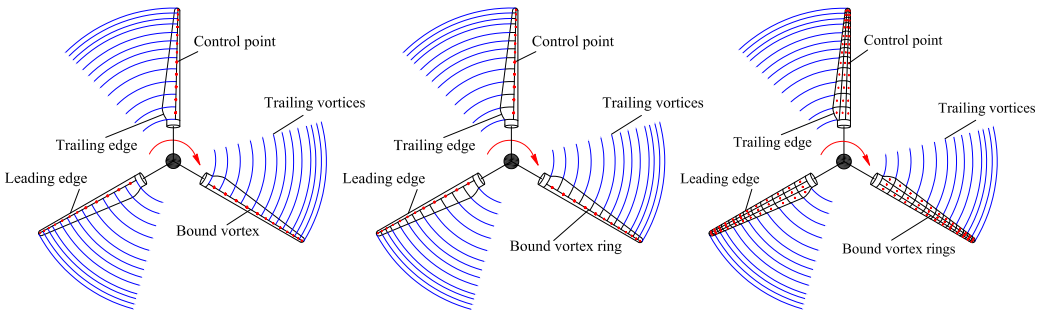


Figure 3.1: *Schematic of different approaches, left: lifting line prescribed wake, middle: lifting surface prescribed wake, right: panel method prescribed wake*

edge follows the helix equation which consists of a helical sheet of vorticity approximated by a series of points connected by a straight vortex filament with a constant diameter and pitch. Hence, there is no wake expansion, and the wake elements move downstream with a constant velocity including free stream and axial induced velocity, where the interaction between the vortex wake filaments is ignored. In the free wake approach, a finite number of vortex wake elements move freely based on the local velocity field, allowing wake expansion as well. Each vortex wake element contains two points, one at the head and another at the tail, which are known as Lagrangian markers. Movement of these vortex wake elements by the local velocity field creates the wake geometry. For both the prescribed and the free wake models, which are based on the inviscid, incompressible and irrotational flow, it is assumed that the trailing wake vortices extend to infinity (Helmholtz's second theorem). However, since the effect of the induced velocity field by the far wake is small on the rotor blade, the wake extends only for a limited length downstream of the wind turbine rotor plane [92].

As stated before, the vortex flow is known as incompressible and inviscid flow. When the blade is modeled as a lifting line, the viscous effect is directly taken into account by using 2D airfoil data, where the generated power and thrust are calculated based on the

lift and drag forces. On the other hand, when the blade is modeled as lifting surface, the power and thrust are calculated based on the potential lift (no viscous drag force) where, in general, the lift coefficient, C_L , is a linear function of the angle of attack, e.g. $C_L = 2\pi(\alpha - \alpha_0)$, according to the thin airfoil theory. This means that the application of lifting surface modeling is limited to attached flow and it must be linked to tabulated airfoil data to predict air loads in the presence of drag and flow separation. Coupling the potential solution of the lifting surface theory to the tabulated airfoil data for wind turbine load calculation will be discussed in Section 3.2.

3.1 Vortex Lattice Free Wake (VLFW)

3.1.1 Modeling

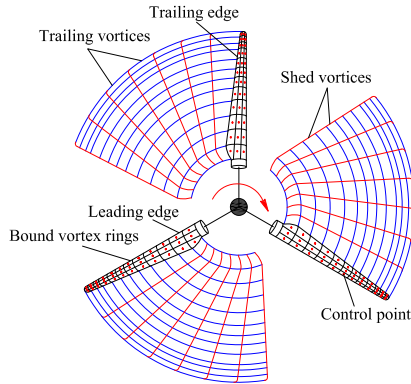


Figure 3.2: *Schematic of vortex lattice free wake*

The vortex lattice method is based on the thin lifting surface theory of vortex ring elements [74], in which the blade surface is replaced by vortex panels that are constructed based on the airfoil camber line of each blade section (see Fig. 3.2). The solution of Laplace's equation with a proper boundary condition gives the flow around the blade resulting in an aerodynamic load calculation, generating power and thrust of the wind turbine. To take the blade surface curvature into account, the lifting surface is divided into a number of panels, both in the chordwise and spanwise directions, where each panel contains a vortex ring with strength $\Gamma_{i,j}$ in which i and j indicate panel indices in the chordwise and spanwise directions, respectively (see Fig. 3.3). The strength of each blade bound vortex ring element, $\Gamma_{i,j}$, is assumed to be constant, and the positive circulation is defined on the basis of the right-hand rotation rule.

In order to fulfill the 2D Kutta condition (which can be expressed as $\gamma_{T.E.} = 0$ in terms of the strength of the vortex sheet where the $T.E.$ subscripts denotes the trailing edge) the leading segment of a vortex ring is located at $1/4$ of the panel length (see Fig. 3.4). The control point of each panel is located at $3/4$ of the panel length meaning that the control point is placed at the center of the panel's vortex ring.

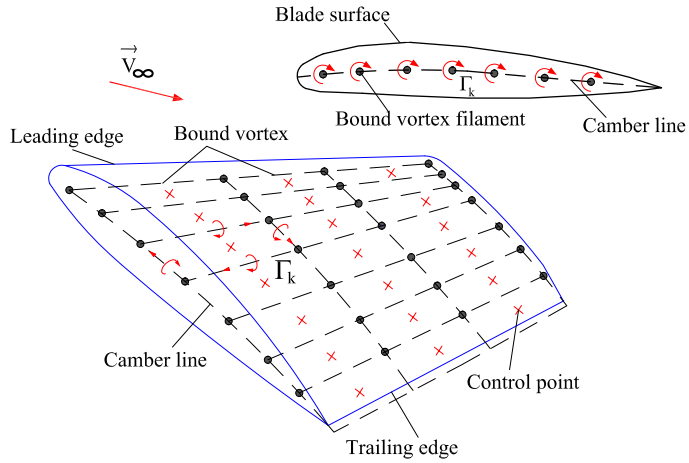


Figure 3.3: *Blade construction using vortex panels*

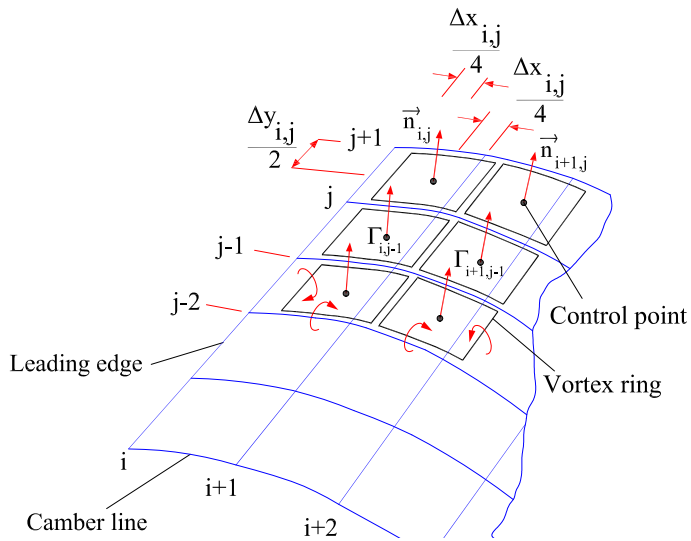


Figure 3.4: *Numbering procedure*

The wake elements which induce a velocity field around the rotor blades are modeled as vortex ring elements, and they are trailed and shed from the trailing edge based on a time-marching method. To satisfy the 3D trailing edge condition for each spanwise section, the strength of the trailing vortex wake rings must be equal to the last vortex ring row in the chordwise direction ($\Gamma_{T.E.} = \Gamma_{Wake}$). This mechanism allows that the blade bound vorticity is transformed into free wake vortices.

To find the blade bound vortices' strength at each time step, the flow tangency condition at each blade's control point must be specified by establishing a system of equations. The velocity components at each blade control point include the free stream (\mathbf{v}_∞), rotational ($\Omega\mathbf{r}$), blade vortex rings self-induced ($\mathbf{v}_{ind,bound}$) and wake induced ($\mathbf{v}_{ind,wake}$) velocities. The blade induced component is known as influence coefficient a_{ij} and is defined as the induced velocity of a j^{th} blade vortex ring with a strength equal to one on the i^{th} blade control point given by

$$a_{ij} = (\mathbf{v}_{ind,bound})_{ij} \cdot \mathbf{n}_i \quad (3.1)$$

If the blade is assumed to be rigid, then the influence coefficients are constant at each time step, which means that the left-hand side of the equation system is computed only once. However, if the blade is modeled as a flexible blade, they must be calculated at each time step. Since the wind and rotational velocities are known during the wind turbine operation, they are transferred to the right-hand side of the equation system. In addition, at each time step, the strength of the wake vortex panels is known from the previous time step, so the induced velocity contribution by the wake panels is also transferred to the right-hand side. Therefore, the system of equations can be expressed as

$$\begin{pmatrix} a_{11} & a_{12} & \cdots & a_{1m} \\ a_{21} & a_{22} & \cdots & a_{2m} \\ \vdots & \vdots & \ddots & \vdots \\ a_{m1} & a_{m2} & \cdots & a_{mm} \end{pmatrix} \begin{pmatrix} \Gamma_1 \\ \Gamma_2 \\ \vdots \\ \Gamma_m \end{pmatrix} = \begin{pmatrix} RHS_1 \\ RHS_2 \\ \vdots \\ RHS_m \end{pmatrix} \quad (3.2)$$

where m is defined as $m = MN$ for a blade with M spanwise and N chordwise panels and the right-hand side is computed as

$$RHS_k = -(\mathbf{v}_\infty + \Omega\mathbf{r} + \mathbf{v}_{ind,wake})_k \cdot \mathbf{n}_k \quad (3.3)$$

The blade bound vortex strength ($\Gamma_{i,j}$) is calculated by solving Eq. (3.2) at each time step. At the first time step (see Figs. 3.5 and 3.6), there are no free wake elements. At the second time step (see Figs. 3.5 and 3.7), when the blade is rotating, the first wake panels are shed. Their strength is equal to the bound vortex circulation of the last row of the blade vortex ring elements (Kutta condition), located at the trailing edge, at the previous time step (see Fig. 3.7), which means that $\Gamma_{W,t_2} = \Gamma_{T.E.,t_1}$, where the W and $T.E.$ subscripts represent the wake and the trailing edge, respectively. At the second time step, the strength of the blade bound vortex rings is calculated by specifying the flow tangency boundary condition where, in addition to the blade vortex ring elements, the contribution of the first row of the wake panels is considered.

This methodology is repeated, and vortex wake elements are trailed and shed at each time step, where their strengths remain constant (Kelvin theorem) and their corner points

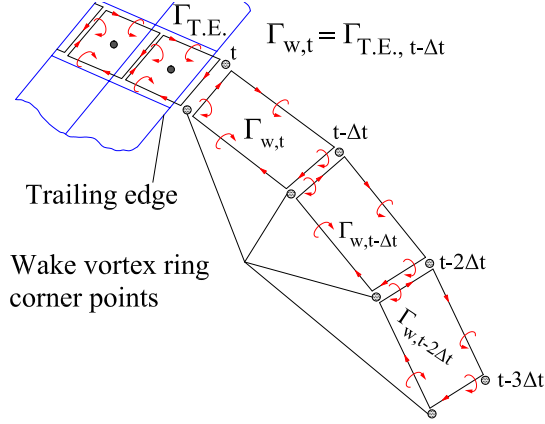


Figure 3.5: *Schematic of generation and moving of wake panels at each time step*

are moved based on the governing equation (see Eq. (3.4)) for the local velocity field, including the wind velocity and the induced velocity by all blades and wake vortex rings. The governing equation for the wake geometry is

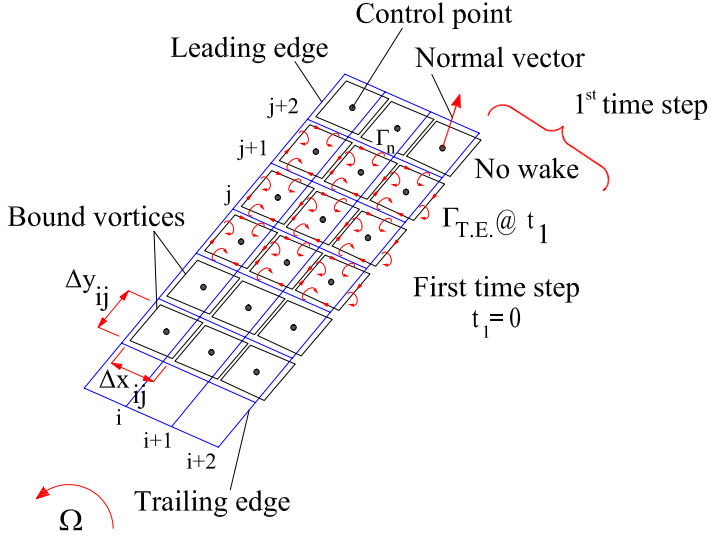


Figure 3.6: *Schematic of wake evolution at the first time step*

$$\frac{d\mathbf{r}}{dt} = \mathbf{v}_{tot}(\mathbf{r}, t) \quad \mathbf{r}(t=0) = \mathbf{r}_0 \quad (3.4)$$

where \mathbf{r} , \mathbf{v}_{tot} and t denote the position of a Lagrangian marker, the total velocity field and time, respectively. The total velocity field, expressed in the rotating reference frame

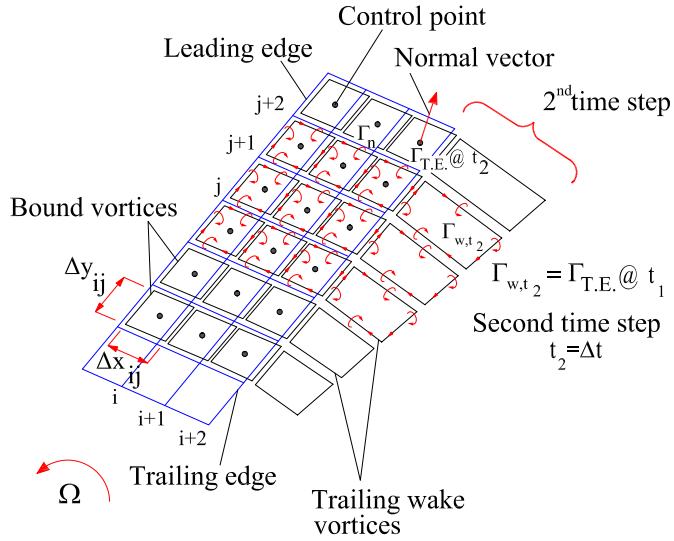


Figure 3.7: Schematic of wake evolution at the second time step

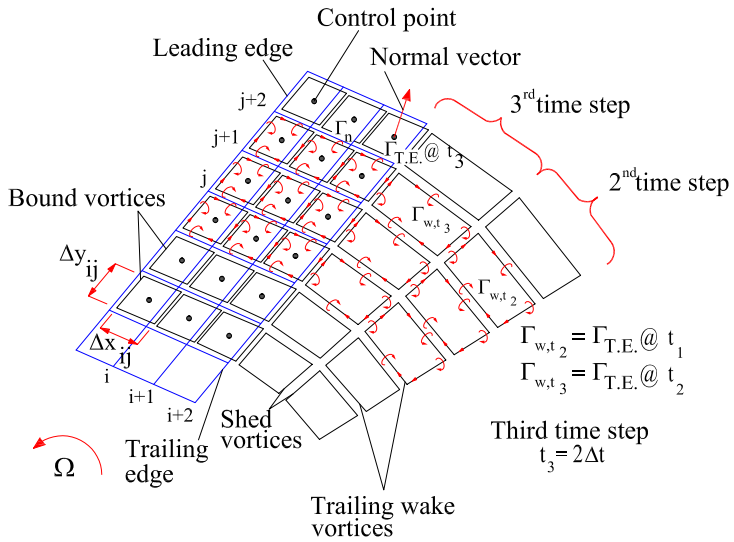


Figure 3.8: Schematic of wake evolution at the third time step

i.e., $\mathbf{v}_{rot} = 0$, can be written as

$$\mathbf{v}_{tot} = \mathbf{v}_{\infty} + \mathbf{v}_{ind,blade} + \mathbf{v}_{ind,wake} \quad (3.5)$$

Different numerical schemes may be used for Eq. (3.4) such as the explicit Euler method, the implicit method, the Adams-Bashforth method and the Predictor-Corrector method. The numerical integration scheme must be considered in terms of the accuracy, stability and computational efficiency. The first-order Euler explicit is given by

$$\mathbf{r}_{t+1} = \mathbf{r}_t + \mathbf{v}_{tot}(\mathbf{r}_t) \Delta t \quad (3.6)$$

where \mathbf{v}_{tot} is taken at the old time step.

According to the linear stability analysis done by Gupta [93], the Euler explicit method is considered to be an unstable integration scheme. Small time steps can be used to improve the stability of this scheme, but the very fine wake discretization, for example 2 – 6 degrees of azimuth, makes the free wake method computationally expensive.

The implicit scheme for a rotor wake application is defined as

$$\mathbf{r}_{t+1} = \mathbf{r}_t + \mathbf{v}_{tot}(\mathbf{r}_{t+1}) \Delta t \quad (3.7)$$

where \mathbf{v}_{tot} is taken at the current time step. The implicit scheme is a stable numerical method. However, since it requires information from the current time step, a set of linear equations must be solved at each time step, making it computationally too expensive and impractical for the free wake method.

Higher order accurate schemes may be also used, such as the 2^{nd} order Adams-Bashforth, reading

$$\mathbf{r}_{t+2} = \mathbf{r}_{t+1} + \frac{1}{2} (3\mathbf{v}_{tot}(\mathbf{r}_{t+1}) - \mathbf{v}_{tot}(\mathbf{r}_t)) \Delta t \quad (3.8)$$

Similar to the Euler explicit method, this scheme is numerically unstable for rotor wake applications [93].

The predictor-corrector scheme is well known as a numerical scheme that improves the stability of the explicit method. In the predictor step, the Euler explicit method is used to get an intermediate solution for the Lagrangian markers' position. The velocity field in the corrector step is then calculated on the basis of the position of Lagrangian markers computed in the predictor step. Mathematically, the predictor step is defined as

$$\tilde{\mathbf{r}}_{t+1} = \mathbf{r}_t + \mathbf{v}_{tot}(\mathbf{r}_t) \Delta t \quad (3.9)$$

and the corrector step becomes

$$\mathbf{r}_{t+1} = \mathbf{r}_t + \mathbf{v}_{tot}(\tilde{\mathbf{r}}_{t+1}) \Delta t \quad (3.10)$$

The drawback of the predictor-corrector scheme is that it requires two velocity field calculations at each time step which accordingly decrease the computational efficiency.

3.2 Load Calculation

In the vortex flow, the only force acting on the rotor blades is the lift force which can be calculated either by Kutta-Jukowski's theory or Bernoulli's equation where the viscous effects such as the skin friction and the flow separation are not included. Therefore, in order to take into account the viscous effects and the flow separation, the potential lift force must be combined with the aerodynamic coefficients through the tabulated airfoil data along with the dynamic stall model to take the unsteady effects into account.

The currently developed VLFW model is based on the thin lifting surface theory of vortex ring elements, where the body is part of the flow domain. Therefore, the effective angle of attack is calculated based on the dynamic approach (force field) by projecting the lift force acting on rotor blades into the normal and tangential directions with respect to the rotor plane. In general, the predicted angle of attack computed on the basis of the potential flow solution (i.e., the lifting surface theory) is always greater than that calculated by the viscous flow. Therefore, it cannot be directly used as entry to look up the tabulated airfoil data to provide the aerodynamic coefficients. This leads us to modify the predicted angle of attack by introducing a method called the 2D static airfoil data method (viscous solution).

In the 2D static airfoil data method, the new angle of attack is calculated by using the tabulated airfoil data where it is directly connected to both the tabulated airfoil data and the potential solution parameter (Γ). This angle of attack is used as the entry to look-up the airfoil table and then we are able to calculate the lift, drag and moment coefficients giving the lift and drag forces for each blade element. It is worth noting that both the standard potential method and 2D static airfoil data method are based on the quasi-static assumption.

In the fully unsteady condition, the lift, drag and moment coefficients are not following the tabulated airfoil data curve (see Appendix A), they need to be corrected and this is done by employing a dynamic stall model. Generally, the aim of the dynamic stall model is to correct the aerodynamic coefficients under the different time-dependent events which were described in the introduction. Hence, in case of uniform, steady inflow condition and in the absence of the blade aeroelastic motion, it is not necessary to use the dynamic stall model.

3.2.1 The Standard Potential Method

In the VLFW method, when the positions of all Lagrangian markers are calculated at each time step, we are able to compute the velocity field around the rotor blade where, as a consequence, the lift force can be calculated according to Kutta-Jukowski's theorem. The differential steady-state form of Kutta-Jukowski's theorem reads

$$d\mathbf{L} = \rho \mathbf{v}_{tot} \times \Gamma d\mathbf{l} \quad (3.11)$$

where ρ , \mathbf{v}_{tot} , Γ and $d\mathbf{l}$ denote the air density, total velocity vector, vortex filament strength and vortex filament length vector, respectively.

Kutta-Jukowski's theorem is applied at the mid-point of the front edge of each blade vortex ring (see Fig. 3.9) and gives the potential lift force where the lift force of each

spanwise blade section is calculated by summing up the lift force of all panels along the chord. In the present work, the lift force for each blade panel is computed using the

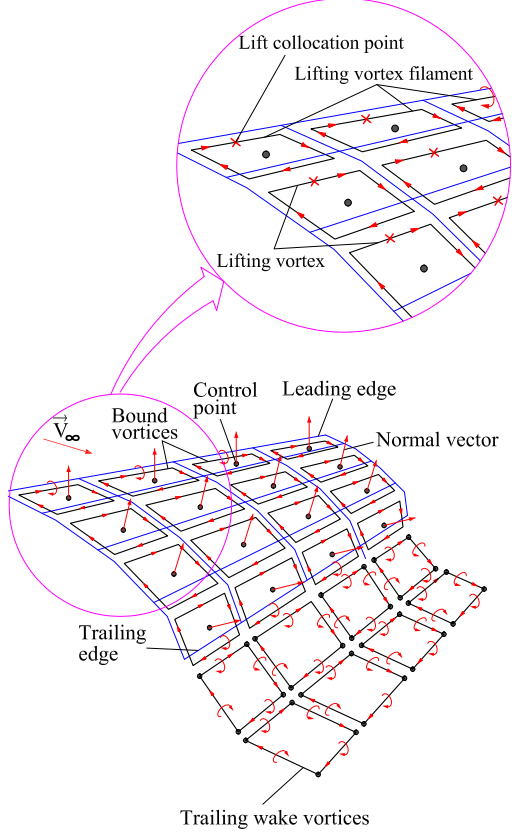


Figure 3.9: *Lift collocation point*

general form of Kutta-Jukowski's theorem given by

$$\mathbf{L}_{i,j} = \rho \mathbf{v}_{tot,i,j} \times (\Gamma_{i,j} - \Gamma_{i-1,j}) \Delta \mathbf{y}_{i,j} + \left(\rho A_{i,j} \frac{\Delta \Gamma_{i,j}}{\Delta t} \mathbf{n}_{i,j} \right) \quad (3.12)$$

where $\Delta \mathbf{y}_{i,j}$, $A_{i,j}$, $\Delta \Gamma_{i,j}/\Delta t$ and $\mathbf{n}_{i,j}$ denote the width vector of a blade vortex panel in the chordwise direction, blade vortex panel area, time-gradient of circulation and unit vector normal to the vortex panel in which i and j indicate panel indices in the chordwise and spanwise directions, respectively. Moreover, $\mathbf{v}_{tot,i,j}$ is computed as

$$\mathbf{v}_{tot,i,j} = \mathbf{v}_{\infty,i,j} + \Omega \mathbf{r}_j + \mathbf{v}_{ind,wake,i,j} + \mathbf{v}_{ind,bound,i,j} \quad (3.13)$$

The second term in Eq. (3.12) is the unsteady term which may be neglected for the steady-state computations. For the blade panels adjacent to the leading edge, Eq. (3.12)

can be written as

$$\mathbf{L}_{1,j} = \rho \mathbf{v}_{tot,1,j} \times \Gamma_{1,j} \Delta \mathbf{y}_{1,j} + \left(\rho A_{1,j} \frac{\Delta \Gamma_{1,j}}{\Delta t} \mathbf{n}_{1,j} \right) \quad (3.14)$$

The total lift of each blade section in the spanwise direction is obtained as

$$\mathbf{L}_j = \sum_{i=1}^N \mathbf{L}_{i,j} \quad (3.15)$$

where N denotes the number of chordwise sections. Decomposition of the lift force for each blade spanwise section into the normal and tangential directions with respect to the rotor plane (see Fig. 3.10) gives the effective potential angle of attack for each section where the angle is computed as

$$\alpha = \tan^{-1} (F_t / F_n) - \theta_t - \theta_p \quad (3.16)$$

where α , F_t , F_n , θ_t and θ_p represent the angle of attack, tangential force, normal force, blade section twist and blade pitch, respectively.

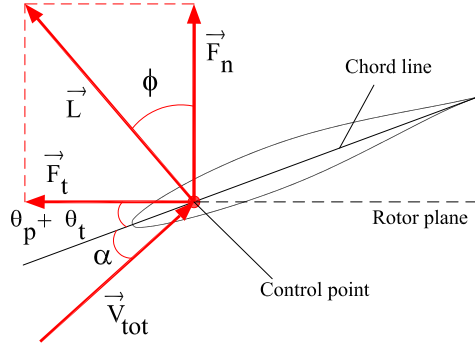


Figure 3.10: *Potential load decomposition*

3.2.2 2D Static Airfoil Data Method

In potential flow, the lift coefficient is expressed by the thin airfoil theory which is a linear function of angle of attack with constant slope equal to 2π . This means that for the thick airfoil, commonly used in wind turbine blades, the thin airfoil theory is no longer valid. In addition, this assumption (linear relation of the lift coefficient and the angle of attack) gives the higher the lift the higher the angle of attack. Hence, considerable lift reduction due to flow separation at higher angles of attack cannot be predicted.

According to Kutta-Jukowski's theory, the magnitude of the lift force per unit spanwise length, L' , is proportional to the circulation, Γ , and it is given by

$$L' = \rho v_{tot} \Gamma \quad (3.17)$$

where ρ , v_{tot} denote the air density and the total velocity magnitude, respectively. The circulation for each spanwise section is equal to the bound vortex circulation of the last row vortex ring element, located at the trailing edge. In addition, in the linear airfoil theory, the lift coefficient is expressed by

$$C_L = m(\alpha - \alpha_0) \quad (3.18)$$

where $m = 2\pi$, α and α_0 indicate the slope, the angle of attack and the zero-lift angle of attack, respectively. The lift coefficient is generally defined as

$$C_L = \frac{L'}{0.5\rho v_{tot}^2 c} \quad (3.19)$$

where c denotes the airfoil chord length. Combination of Eqs. (3.17), (3.18) and (3.19) gives the modified angle of attack as

$$\alpha = \frac{2\Gamma}{mV_{tot}c} + \alpha_0 \quad (3.20)$$

For an arbitrary airfoil, both m and α_0 are determined according to the C_L vs. α curve where the constant lift coefficient slope, m , is computed over the linear region (attached flow). The modified angle of attack based on the Eq. (3.20) is used as entry to calculate the lift, the drag and the moment coefficients through the tabulated airfoil data. As

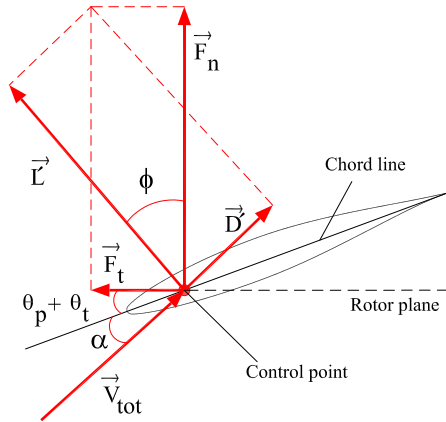


Figure 3.11: *Viscous load decomposition*

a result, the lift and drag forces are computed for each blade element in the spanwise section giving the tangential and normal forces acting on the rotor blade (see Fig. 3.11).

3.2.3 Dynamic Stall Method

The semi-empirical dynamic stall model, called the Extended ONERA is used to predict the unsteady lift, drag and moment coefficients for each blade spanwise section based on

2D static airfoil data. In this model, the unsteady airfoil coefficients are described by a set of differential equations including the excitation and the response variables, where they are applied separately for both the attached and separated flows.

In the initial version of the ONERA model, the excitation variable is the angle of attack with respect to the chord line whereas in the extended version, the excitation variables are W_0 and W_1 , the velocity component perpendicular to the sectional chord and the blade element angular velocity for the pitching oscillation, respectively.

Furthermore, compared with the initial version of the ONERA model, in the extended model, instead of the lift coefficient (C_L), the circulation (Γ) which is responsible for producing lift is the response variable. Also, the variation of the wind velocity is included in the extended model which does not exist in the early version [94].

In the extended ONERA model, the lift (L) and the drag (D) forces are written as

$$L = \frac{\rho c}{2} \left[v_{tot} (\Gamma_{1L} + \Gamma_{2L}) + \frac{S_L c}{2} \dot{W}_0 + \frac{K_L c}{2} \dot{W}_1 \right] \quad (3.21)$$

and

$$D = \frac{\rho c}{2} \left[v_{tot}^2 C_{D,Lin} + \frac{\sigma_D c}{2} \dot{W}_0 + v_{tot} \Gamma_{2D} \right] \quad (3.22)$$

where the symbol ($\dot{}$), ρ , c , v_{tot} , Γ_{1L} , Γ_{2L} , W_0 , W_1 , Γ_{2D} and $C_{D,Lin}$ denote the derivation with respect to time, air density, blade element chord length, total velocity, linear circulation related to the attached flow lift, non-linear circulation related to the separated flow lift, total velocity component perpendicular to the sectional chord, rotational velocity of the blade section due to the pitching oscillation, non-linear circulation related to the separated flow drag and linear drag coefficient, respectively. For detailed description of other coefficients in Eqs. (3.21) and (3.22), see Appendix A.

4 Summary of papers

A brief summary of all publications presented in the appended papers is introduced in this chapter.

4.1 Paper A

”Vortex method application for aerodynamic loads on rotor blades”

4.1.1 Summary

In this paper different blade models such as a lifting line method, a lifting surface method (one bound vortex ring) and a panel method (several bound vortex rings) with prescribed wake model were studied for wind turbine aerodynamics. For the lifting line and lifting surface methods, the prescribed wake was introduced as horseshoe trailing vortices while for the lifting panel method, it was constructed by vortex ring elements. For the steady-state operating condition, the vortex ring elements are converted to the horseshoe trailing vortices since there is no shed vortices (time-varying vortex wake elements). The aim was to investigate the impact of blade and wake models on the aerodynamic loads together with computational time efficiency. Because of the prescribed wake modeling, an iterative method was employed to update the initialized helical vortex wake sheet (based on the axial and circumferential velocities) generated by spanwise bound circulation difference along the rotor blades. The 5-MW reference wind turbine was used under the steady-state free stream and constant rotational velocity. The results of different approaches were compared with the GENUVP code. The predicted forces by the lifting line method showed a better agreement than those by the lifting surface and panel methods. This may reflect the impact of the blade modeling on the generated power and thrust of a wind turbine. Moreover, the normal and tangential forces were poorly predicted by the lifting surface method because of neglecting the blade surface curvature.

4.1.2 Comments

It was concluded that the lifting line method predicts better circulation distribution along the blade than the panel method since it is directly linked to the tabulated airfoil data; the properties of each blade section airfoil are taken into account. However, in the panel method, there is no relation between the blade profile properties and circulation distribution along the blade obtained by imposing the zero-normal flow boundary condition. This conclusion must be modified; since the panel method is based on the thin lifting surface theory assuming a constant lift-curve slope equal to 2π per radian representing the physical properties of each blade section airfoil. Since all calculations were done in the global coordinate system (non-rotating frame), V_{rel} must be changed to V_{tot} . Instead of the cut-off radius method, the viscous core model for correction of Biot-Savart’s law is recommended.

4.2 Paper B

”Development of free vortex wake method for aerodynamic loads on rotor blades”

4.2.1 Summary

The outcomes of the previous paper gave an insight to choose a proper combination of the rotor blade and wake models with less restriction and more accuracy. This led us to develop a vortex lattice free wake (VLFW) method. Recall that in the VLFW model, the blade is modeled as a lifting panel method which is equivalent to a lifting surface method including several bound vortex rings both in the chordwise and spanwise directions; the vortex wake elements emanating from the blades’ trailing edge move freely based on the local velocity field. The developed time-marching VLFW model was used to calculate the air loads for 5-MW reference wind turbine while it was assumed that the upstream flow is uniform both in time and space, parallel to the rotating axis; the blades were rigid. The results were compared with the BEM method, the GENUVP code and the CFD simulation made by the RANS (Reynolds-Averaged Navier-Stokes) solver. The first-order Euler explicit numerical scheme was applied for the motion of the Lagrangian markers. The angle of attack, normal and tangential forces along the blade were computed by decomposing the potential lift force, given by Kutta-Jukowski’s theory, for each blade spanwise section; they were compared with the above mentioned approaches. Apart from the BEM method, the VLFW model is more efficient than CFD in terms of the simulation time which makes it apt for wind turbine load calculations. The predicted power by the potential VLFW model was higher than the BEM and CFD methods as expected. The difference between the power predicted by the VLFW method (as potential flow) and CFD (as viscous flow) led us to couple the potential based solution of the VLFW model to tabulated airfoil data to predict air loads in the presence of drag and flow separation.

4.2.2 Comments

In page 3 of paper B, the numerator of correction factor K_v for Biot-Savart’s law in Eq. (5) must be modified by replacing h^n by h^2 . It is also recommended to employ the new correction factor proposed by Van Hoydonck (see Chapter 2). The simulation time for the GENUVP code must be revised from 5.6 [hr] to 2 [hr].

4.3 Paper C

”Development of free vortex wake method for yaw misalignment effect on the thrust vector and generated power”

4.3.1 Summary

Deviation of thrust vector relative to the generator shaft is known as one of the vibration sources for a wind turbine in large yaw misalignment. The main purpose of this paper was to study the deviation of thrust vector relative to rotor shaft for different yaw

misalignments and wind speeds. The developed time-marching vortex lattice free wake (VLFW) and BEM methods were used for the simulations, and the results were validated against the measurement data provided for a two-bladed variable speed machine. The wind speed varied for each inflow direction deviated between -20 and 20 degrees with respect to the rotor axis. The mean wind shear exponent was also extracted from the experiments depending on the mean wind speed. Among different engineering methods modifying the BEM method for yawed flow, the skewed wake geometry with trailing vortices method was employed in the implemented BEM code. This method, which is a function of blade azimuthal angle, gives the skewed axial induction factor as the average of axial induction factor through a rotor revolution. In the VLFW model, the aerodynamic forces were calculated using the standard potential method and 2D static airfoil data method, based on the quasi-static assumption. The lift force and angle of attack were computed by the standard potential method for each blade section according to Kutta-Jukowski's theorem where the viscous effects such as the skin friction and the flow separation were not included. The major application of the 2D static airfoil data method was to modify the angle of attack obtained from the standard potential method. Contrary to the standard potential method, this modified angle of attack can be used as the entry to look-up the airfoil table providing the lift and drag forces for each blade element. The results showed that the 2D static airfoil data method might predict more accurate results (thrust angle and generated power) than the standard potential method and the BEM method with respect to the measurements. In addition to the yaw misalignment making load imbalance over the turbine, vertical wind shear gives rise to cyclic variation with period of 1P in the angle of attack. Lastly, the predicted power and thrust angle deviation for the identical positive and negative yawed flows were not the same due to the rotation direction of the rotor blades.

4.3.2 Comments

In the simulations made with the BEM method, the axial induction factor was only corrected due to the yawed flow while the vertical wind shear was directly accounted for each blade element. In the BEM implementation for sheared inflow, additional correction for axial induction factor (as a function of azimuthal position and radial position of blade elements) on the basis of local thrust coefficient must be taken into consideration. This means that the simulation made with the BEM method must be revised including the correction of axial induction factor for both the yaw misalignment and wind shear. In the VLFW method, the lift force was calculated by the steady-state formulation of Kutta-Jukowski's theory whereas the yawed flow and sheared inflow make an unsteady environment for a wind turbine. It is recommended to compute the potential lift force on the basis of the unsteady formulation of Kutta-Jukowski's theory to take the impact of shed vortices on the total lift force into account, even if the upstream flow is steady in time. Moreover, the 2D static airfoil data method must be modified in order to take the impact of the separation point on the trailing and shed vortices into account. This may be done using an iterative method the so-called decambering approach for the post-stall prediction.

4.4 Paper D

”Numerical studies of the upstream flow field around a horizontal axis wind turbine”

4.4.1 Summary

The principal laws behind the BEM method are the ideal horizontal axis wind turbine with wake rotation and 1D ideal rotor disc theories, respectively. These theories could only estimate the axially and the tangentially induced velocities at the rotor plane; and they can predict neither the induced velocity field upstream the rotor plane nor the radial induced velocity. The impact of the axially induced velocity upstream the rotor plane is to reduce a power reduction of the wind turbine. In this paper, the developed time-marching VLFW code was used to study the impact of the rotor blade azimuthal position, on upstream and downstream flow field near to the rotor plane. For this purpose, the 3-bladed MEXICO wind turbine was used in the simulation and the results were compared with the wind tunnel measurements. The velocity field was measured using the PIV techniques for radial traverses in the horizontal plane, both upstream and downstream of the rotor at different blade positions while the free stream was set to be uniform, steady and perpendicular to the rotor plane. Overall, there was a good agreement between the simulation and experiments while a constant difference between the calculated axial velocity profile by the simulation and measurement data was referred to a reduction of the streamwise velocity due to the open type wind tunnel employed in the measurements. Downstream of the rotor blade, an abrupt change in the axial velocity component in the blade tip region was reported due to the presence of the tip vortex varying with respect to the azimuthal angle. The tip vortex position downstream of the rotor blades, corresponded to the radial position of minimum axial velocity, was fairly well predicted by the simulation. Apart from the negligible radial velocity component upstream the rotor, the small radial velocity component downstream of the rotor was introduced as the main source of the wake expansion which was verified by both the simulation and measurements.

4.4.2 Comments

Although the turbine’s nacelle was not modeled in the VLFW simulation, it did not affect the results since the PIV sheet position was not located at the nacelle’s wake. This means that the effect of the nacelle is limited only for a certain length downstream the rotor, but it is recommended to model the nacelle in the VLFW code.

4.5 Paper E

”Development of free vortex wake model for wind turbine aerodynamics under yaw condition”

4.5.1 Summary

This paper aims to study the effect of the skewed wake, due to a yaw misalignment, on the wake aerodynamics of a horizontal axis wind turbine. An asymmetrical attribute of the yaw misalignment changes significantly the velocity field around the rotor blades making a periodic load variation along the rotor blade which accordingly increases the fatigue load. Moreover, the yaw misalignment makes a time varying and 3D aerodynamic environment for a horizontal axis wind turbine because of the advancing and retarding effect. The advancing and retarding effect occurs due to the lateral component of the incoming velocity where the inflow at the rotor blade depends on the blade azimuthal position. It also makes a temporal variation of the circulation around the blade section which in turn influences the induced velocity field, even if the upstream flow is steady and uniform. The simulations were made by the time-marching VLFW code where the results were compared with the MEXICO wind turbine measurements. A preliminary study was done to choose a suitable vortex core size employed in the free wake simulation. For this purpose, the effect of the vortex core radius on the radial and axial streaklines was investigated while the upstream flow was assumed to be steady and uniform (non-yawed condition). It was found that, contrary to a large vortex core size, a small vortex core size does not delay the vortex roll-up. However it makes the trailing wake vortices to deflect earlier which consequently increases the wake instability. Comparing the radial and axial streaklines of both non-yawed and yawed flows revealed that the trailing wake does not expand symmetrically for the yawed flow which is in contrast to the non-yawed flow. In addition, yaw misalignment makes the trailing wake to evolve periodically. According to the MEXICO experiments, the velocity field was shown for the radial and axial traverses, both upstream and downstream of the rotor. There was a good agreement between the simulations and measurements for the tangential (u) and axial (w) velocities along the radial traverses. A poor agreement for the radial velocity (v) indicated that the rotational effects on the wake aerodynamics of a wind turbine were not well captured by the vortex method. It was also observed that the induction effect of the rotor blades on the radial traverses is small both upstream and downstream except for the radial velocity component which made the wake to expand radially. A significant change downstream of the rotor for both axial and tangential velocities was reported due to the presence of the tip vortex. Different signs and magnitudes of the tangential velocity along the downstream radial traverse verified that the trailing wake expanded laterally and asymmetrically with larger expansion downwind of the rotor plane rather than upwind of the rotor. The radial tip vortex position downstream of the rotor blades verified the smaller wake expansion for the yawed condition, close to the rotor plane, than for the non-yawed condition. There was a good agreement between the simulation and measurement for the axial traverses except for the regions where the turbine's nacelle was not modeled. Apart from the radial expansion of the trailing wake due to the positive magnitude of the radial velocity after the rotor center, the behavior of the tangential velocity downstream of the rotor plane indicated an unequal expansion and deflection of the wake moving forward. Further, the periodic evolution of the trailing wake made the tangential velocity downstream of the rotor plane to oscillate.

4.5.2 Comments

In page 6 of the paper, in the last paragraph and the second line of the end, **IJ** must be changed to **KL**. It is also recommended to include the nacelle in the study of wind turbine wake aerodynamics.

4.6 Paper F

”Enhancement of free vortex filament method for aerodynamic loads on rotor blades”

4.6.1 Summary

In this paper three different aerodynamic load calculation methods, namely standard potential method (potential solution), 2D static airfoil data model (viscous solution) and dynamic stall model were implemented in the Vortex Lattice Free Wake (VLFW) code. The aim was to increase capability of the potential solution of the free vortex wake method to predict viscous phenomena such as drag and separation using the tabulated airfoil data. Predicted normal and tangential forces using the VLFW method were compared with the Blade Element Momentum (BEM) method, the GENUVP code and the MEXICO wind tunnel measurements. In the VLFW code, the lift force was calculated by Kutta-Jukowski’s theory. The effective angle of attack was then computed by projecting the lift force into the normal and tangential directions with respect to the rotor plane. However, the predicted angle of attack could not be directly used as entry to look up the tabulated airfoil data to provide the aerodynamic coefficients since it was obtained from the potential flow solution. A remedy was to introduce a method called the 2D static airfoil data method (viscous solution) to modify the predicted angle of attack calculated by the standard potential method. This modification was achieved by combining both the tabulated airfoil data and the potential solution parameter (Γ). Moreover, a semi-empirical model, called the Extended ONERA model was added to the VLFW code to account for the dynamic stall effects due to unsteady conditions. Two different turbines, NREL and MEXICO, were used in the simulations to validate different load calculation methods implemented in the VLFW code. For the NREL 5-MW machine, in addition to the power and thrust curves, the angle of attack and tangential force along the rotor blade were studied and they were compared with the BEM method and the GENUVP code. For the MEXICO turbine, two different steady inflow conditions (with and without yaw misalignment) were employed in the VLFW simulations. The tangential and normal forces acting on the rotor blades were compared with the existing experimental data. The VLFW simulation for both the MEXICO and the NREL 5-MW turbines showed that this method (vortex method) can be used as a suitable engineering method for wind turbine’s aerodynamics covering a broad range of operating conditions. For the non-yawed flow, apart from a rather good agreement between the VLFW simulation and the MEXICO measurement in terms of the tangential and normal forces along the blade, domination of the viscous phenomena such as flow separation and stall condition for the higher freestream velocities made the potential flow assumption less accurate. This certified the necessity of coupling the 2D static airfoil data to the standard potential method for more accurate loads and power

prediction. For the yawed flow, the aerodynamic forces normal and parallel to the local chord as a function of azimuthal position for the five radial stations along blade 1 were compared with the MEXICO measurements. The potential solution and the measurement data showed almost the same trend although the VLFW method overpredicted azimuthal variation of the tangential and normal forces. Although the viscous solution made a slight improvement in terms of magnitude of the tangential and normal forces, it could not predict the trends, especially for the tangential force in the blade root region. However, the dynamic stall solution made adjustment between the potential and viscous solutions. The large offset between the simulation and the measurement was reported due to the poor quality of the interpolated airfoil profile located at the transition region between the Risø and NACA airfoils (0.6R). The VLFW simulations displayed a phase shift (at almost all spanwise sections) compared with the experiments for both the normal and tangential forces.

4.6.2 Comments

A deficiency in the streamwise velocity due to open type wind tunnel employed in the experimental investigation has been reported. It is recommended to make the VLFW simulation by taking the tunnel effect into account. As described in the paper, all parameters for the dynamic stall method were chosen on the basis of the flat plate and mean profile values since no wind tunnel measurement data founded for different airfoil profiles constructing the MEXICO turbine's rotor.

4.7 Paper G

"Assessment of the influence of turbulent inflow fields on wind turbine power production"

4.7.1 Summary

The effect of the turbulent inflow on the power production of a horizontal axis wind turbine was studied in this paper. For this purpose, three different inflow methods, i.e. a time series of atmospheric atmospheric boundary layer flow field (TS), Taylor's hypothesis (TH) and a steady-state mean wind profile with shear (PL) over a forest region and over a flat terrain with low aerodynamic roughness (non-forest region) were employed. The free vortex wake (VLFW) code was used to predict the aerodynamic loads for the NREL 5-MW turbine. Apart from the steady-state wind profile provided by the PL method, the turbulent wind fields, TS and TH methods, were extracted from Large-Eddy Simulation (LES) and synthetic turbulence (Mann model), respectively. In all three different inflow methods, a constant mean speed was specified at the hub height for both forest and non-forest regions. Furthermore, validity of Taylor's hypothesis was investigated for both forest and non-forest regions since its application is limited to flows with low turbulence intensity. In the TS method, LES was used for simulating the atmospheric boundary layer over a 20 [m] high, horizontally homogeneous forest region and over a non-forest region while neutral stratification and periodic boundaries in the horizontal directions were assumed. In LES, the incompressible, grid-filtered Navier-Stokes equations were

solved where the influence of the forest canopy and the Coriolis effect were introduced as the source terms in the momentum equation. Additionally, a transport equation for SGS turbulent kinetic energy (TKE) was solved to provide a velocity scale for modeling the smallest eddies. In the TH method, a single three-dimensional wind field from synthetic turbulence (Mann model) was generated where different input parameters were specified for the non-forest and forest regions, respectively. In the PL method, the wind profile was determined by the power law where the shear exponents were extracted over the rotor area obtained from the LES for the non-forest and forest regions. Because of the time varying turbulent inflow condition employed by the VLFW model based on the TS method, various azimuthal resolutions for the wake segmentation were tested. The mean and the standard deviation of power production were compared for different azimuthal rotor increments resulting in the 10° resolution to satisfy both accuracy and computational efficiency. The smaller mean power was predicted by the TH and PL methods with respect to the TS method for both non-forest and forest regions while the presence of forest canopies reduced the mean power as well. Recall that the generated wind field by both LES and synthetic turbulence in the forest region had the same turbulence intensity at the hub height. The smaller prediction of mean power by the TH method than the TS method led us to investigate the application of Taylor's hypothesis for flows with high turbulence intensity. Despite the slightly lower standard deviation of fluctuating power in the forest region, the PL method predicts the same mean power for forest and non-forest regions which is inconsistent with the results of turbulent flow fields. The results showed that the presence of the forest canopies increases the standard deviation of the turbine's fluctuating power giving rise to a higher level of fatigue loads. Moreover, because of the higher turbulent kinetic energy (TKE) generated by LES, the standard deviation of fluctuating power for the TS method was larger than the TH method. The histogram of the fluctuating power production for the turbulent inflow methods showed that the forest canopies increase the deviation of the instantaneous power production with respect to the mean power. In addition, the effect of the forest region on the time varying power production and the oscillating angle of attack for each spanwise section were more pronounced for the TS method than the TH method. Validity of Taylor's hypothesis was additionally studied using the local convective velocity based on the cross correlating (space-time correlation) of the fluctuating velocities at two arbitrary grid points which were axially separated by a specified distance. The computed convective velocity exceeded the mean velocity for the forest region increased the ambiguity of Taylor's hypothesis application for flows with high turbulence intensity. Moreover, the TH method was employed using a number of boxes which were deliberately chosen among the 300 different synthetic turbulent fields (identical input parameters but using different seeds for the random generation). Contrary to the non-forest region, no distinctive pattern was observed to describe the variation of mean power with respect to the turbulence level of flow field. This might be translated into the uncertainty of using the TH method to study the influence of turbulent inflow fields on wind-turbine power production, especially for the regions with high turbulent intensity such as the forest canopies.

4.7.2 Comments

It is recommended to make the VLFW simulation for more rotor revolutions to analyze dependency of the inflow turbulence and power production of a wind turbine. Likewise it is recommended to study the effect of forest canopies with different densities on mean power production.

5 Concluding Remarks

The aim of the project was to develop a vortex-based computational method for predicting unsteady aerodynamic loads on wind turbine rotor blades. Among different blade models such as a lifting line method, a lifting surface method and a panel method with either prescribed or free wake model, it was found out that a combination of the panel method (as rotor blade) and the free wake method the so-called vortex lattice free wake (VLFW) method is the most accurate method. This led us to focus on developing a time-marching VLFW method as the inviscid, incompressible and irrotational flow where its potential solution was coupled to tabulated airfoil data and a semi-empirical model to take into account the viscosity and the dynamic stall effects, respectively. The implemented VLFW method was validated against the BEM and CFD methods, the GENUVP code by National Technical University of Athens (NTUA), Hönö turbine measurement data and MEXICO wind tunnel measurements where a quite good agreement was obtained.

It was determined that the accuracy of the VLFW model significantly depends on some geometrical parameters such as the blade discretization (both spanwise and chordwise sections), the discretization of the wake elements and the wake truncation length. In the panel method the blade surface was constructed based on the airfoil camber line of each blade section. A blade might be also modeled by a full panel method (including full airfoil profile of each blade section) which provides more flow details around the rotor. However, for load calculations, a camber line-based panel method gave satisfactory results in terms of both accuracy and computational time efficiency. In addition, choosing an appropriate vortex core size employed in the correction factor of Biot-Savart's law was crucial for evolution of the trailing wake vortices, especially for turbulent and yawed inflows.

Employing the unsteady form of Kutta-Jukowski's theory was necessary to take the impact of shed vortices on the total potential lift force into account. It was shown that the 2D static airfoil data method could remarkably modify the angle of attack obtained from the standard potential method even though both of them were based on the quasi-static assumption. It was also found out that an iterative method the so-called decambering approach for the post-stall prediction could provide better approximation for viscous effects than the 2D static airfoil data method. The adjustment role of the semi-empirical dynamic stall method (between the potential and viscous solutions) the so-called Extended ONERA model works quite well.

The results showed that the nacelle affected the air flow downstream the rotor for a certain length which motivated to include the nacelle in the study of wake aerodynamics. This led us to include a tower shadow model as well in future development of the VLFW code.

The VLFW method was successfully used to study the influence of turbulent inflow fields, extracted from either Large-Eddy Simulation (LES) or synthetic turbulence (Mann model), on wind turbine power production. Because of the inflow's turbulent fluctuations, a chaotic motion of straight vortex wake filaments was observed while the impact of vortex filaments stretching was neglected. Generally, a vortex filament stretching changes the vortex core radius which accordingly affects the velocity induced by a vortex wake element. A remedy is either to subdivide a vortex filament into two vortex filaments when it is stretched beyond a specified length (constant vortex core size approach) or

to modify the vortex core radius based on the strain rate over a specified time period (varying vortex core size). Taking a vortex filament stretching into account improves the evolution of free vortex wake elements, however it increases the computational time.

In all prescribed and free wake models in this work, the blade was assumed to be rigid. Nevertheless, the elastic deformation of rotor blades influences the wind turbine performance. Hence, coupling the VLFW code into an aeroelastic solver would be necessary. It is also worth mentioning that the developed VLFW code could handle all sorts of temporal and spatial movements of components such as blade pitch regulation, cone angle, shaft tilt and etc. which may be used for future studies.

References

- [1] H. Abedi, L. Davidson, and S. Voutsinas. “Vortex method application for aerodynamic loads on rotor blades”. *EWEA 2013 Conference*. Vienna, Austria, 4–7 February, 2013.
- [2] H. Abedi, L. Davidson, and S. Voutsinas. “Development of free vortex wake method for aerodynamic loads on rotor blades”. *EWEA 2014 Conference*. Barcelona, Spain, 10–13 March, 2014.
- [3] H. Abedi, L. Davidson, and S. Voutsinas. “Development of free vortex wake method for yaw misalignment effect on the thrust vector and generated power”. *32nd AIAA Applied Aerodynamics Conference*. AIAA Aviation paper 2014-2847. Atlanta, GA, United States, 16–20 June, 2014.
- [4] H. Abedi, L. Davidson, and S. Voutsinas. “Numerical studies of the upstream flow field around a horizontal axis wind turbine”. *33rd Wind Energy Symposium*. AIAA SciTech paper 2015-0495. Kissimmee, FL, United States, 5–9 January, 2015.
- [5] H. Abedi, L. Davidson, and S. Voutsinas. “Development of free vortex wake model for wind turbine aerodynamics under yaw condition”. *34th Wind Energy Symposium*. AIAA SciTech paper 2016-1257. San Diego, CA, United States, 4–8 January, 2016.
- [6] H. Abedi, L. Davidson, and S. Voutsinas. Enhancement of free vortex filament method for aerodynamic loads on rotor blades. *Submitted to Journal of Solar Energy Engineering* (2016).
- [7] H. Abedi, B. Nebenführ, L. Davidson, and S. Voutsinas. Assessment of the influence of turbulent inflow fields on wind-turbine power production. *to be submitted to a scientific journal* (2016).
- [8] W. J. M. Rankine. *On The Mechanical Principle of the Action of Propellers*. Transactions of the Institute of Naval Architects. Vol. 6, 1865.
- [9] W. Froude. *On The Elementary Relation between Pitch, Slip and Propulsive Efficiency*. Transactions of the Institute of Naval Architects. Vol. 19, 1978.
- [10] M. O. L. Hansen. *Aerodynamics of Wind Turbines*. 2nd edition. EarthScan, 2008.
- [11] J. N. Sørensen. *General Momentum Theory for Horizontal Axis Wind Turbines*. Springer International Publishing Switzerland, 2016.
- [12] A. van Garrel. *Development of a Wind Turbine Aerodynamics Simulation Module*. ECN report, ECN-C-03-079, August 2003.
- [13] L. J. Vermeer, J. N. Sørensen, and A. Crespo. Wind Turbine Wake Aerodynamics. *Progress in Aerospace Sciences* **39** (2003), pp. 467–510.
- [14] H. Glauert. *The Elements of Airfoil and Airscrew Theory*. University Press, Cambridge, 1948.
- [15] W. F. Durand. *Aerodynamic Theory, A General Review of Progress Under a Grant of the Guggenheim Fund for the Promotion of Aeronautics, Volume IV*. Springer Berlin Heidelberg, 1935.
- [16] L. Prandtl. *Application of Modern Hydrodynamics to Aeronautics*. NACA Report 116. 1921.
- [17] S. Goldstein. “On the Vortex Theory of Screw Propellers”. *Proceedings of the Royal Society of London*. Vol. 123.

- [18] V. M. Falkner. *The Calculation of Aerodynamic Loading on Surfaces Of any Shape*. British Aeronautical Research Council. 1943.
- [19] V. L. Okulov and J. N. Sørensen. Maximum efficiency of wind turbine rotors using Joukowsky and Betz approaches. *Journal of Fluid Mechanics* **49** (2010), pp. 497–508.
- [20] V. L. Okulov, J. N. Sørensen, and D. H. Wood. Rotor theories by Professor Joukowsky: Vortex theories. *Progress in Aerospace Sciences* **73** (2015), pp. 19–46.
- [21] J. N. Sørensen and G. A. M. van Kuik. General momentum theory for wind turbines at low tip speed ratios. *Journal of Wind Energy* **14**(7) (2011), pp. 821–839.
- [22] V. L. Okulov and G. A. M. van Kuik. The Betz-Joukowsky limit: on the contribution to rotor aerodynamics by the British, German and Russian scientific schools. *Journal of Wind Energy* **15**(2) (2012), pp. 335–344.
- [23] G. A. M. van Kuik, J. N. Sørensen, and V. L. Okulov. Rotor theories by Professor Joukowsky: Momentum theories. *Progress in Aerospace Sciences* **73** (2015), pp. 1–18.
- [24] D. G. Opoku, D. G. Triantos, F. Nitzsche, and S. G. Voutsinas. “Rotorcraft Aerodynamic and Aeroacoustic Modeling using Vortex Particle Methods”. In *Proceedings of the 23rd International Congress of the Aeronautical Sciences, ICAS, Toronto, Canada*. 2002.
- [25] S. G. Voutsinas, M. A. Beleiss, and K. G. Rados. “Investigation of the Yawed Operation of Wind Turbines by means of a Vortex Particle Method”. *AGARD Conference Proceedings*. Vol. 552. 1995, pp. 11.1–11.
- [26] J. Zhao and C. He. A Viscous Vortex Particle Model for Rotor Wake and Interference Analysis. *Journal of the American Helicopter Society* **55**(1) (2010), p. 12007.
- [27] T. A. Egolf. “Helicopter Free Wake Prediction of Complex Wake Structures Under Blade-Vortex Interaction Operating Conditions”. In *Proceedings of the 44th Annual Forum of the American Helicopter Society, Washington, DC*. 1988, pp. 819–832.
- [28] A. Rosen and A. Graber. Free Wake Model of Hovering Rotors Having Straight or Curved Blades. *Journal of the American Helicopter Society* **33**(3) (1988), pp. 11–21.
- [29] S. Gupta. *Development of a Time-Accurate Viscous Lagrangian Vortex Wake Model for Wind Turbine Applications*. University of Maryland, Department of Aerospace Engineering, 2006.
- [30] S. D. Pasmajoglou and J. M. R. Graham. Prediction of Aerodynamic Forces on Horizontal Axis Wind Turbines in Free Yaw and Turbulence. *Journal of Wind Engineering and Industrial Aerodynamics* **86** (2000), pp. 1–14.
- [31] S. G. Voutsinas. Vortex Methods in Aeronautics: How to Make Things Work. *International Journal of Computational Fluid Dynamics* **20** (2006), pp. 3–18.
- [32] J. J. Chattot. Helicoidal Vortex Model for Wind Turbine Aeroelastic Simulation. *Computers and Structures* **85** (2007), pp. 1072–1079.
- [33] J. J. Chattot. Optimization of Wind Turbines using Helicoidal Vortex Model. *Journal of Solar Energy Engineering* **125** (2003), pp. 418–424.
- [34] J. G. Holierhoek, J. B. de Vaal, A. H. van Zuijlen, and H. Bijl. Comparing Different Dynamic Stall Models. *Journal of Wind Energy* **16** (2013), pp. 139–158.
- [35] A. J. Landgrebe. The Wake Geometry Of a Hovering Rotor and its Influence on Rotor Performance. *Journal of the American Helicopter Society* **17**, No. 4 (1972), pp. 2–15.

- [36] J. D. Kocurek and J. L. Tangler. A Prescribed Wake Lifting Surface Hover Performance Analysis. *Journal of the American Helicopter Society* **22(1)** (1977), pp. 24–35.
- [37] T. A. Egolf and A. J. Landgrebe. Helicopter Rotor Wake Geometry and its Influence in Forward Flight, Vol. 1 Generalized Wake Geometry and Wake Effects in Rotor Airloads and Performance. *NASA CR-3726* (1983).
- [38] A. J. Landgrebe. *An Analytical and Experimental Investigation of Helicopter Rotor Hover Performance and Wake Geometry Characteristics*. USAAMRDL Tech. Report 71-24, US Army Air Mobility Research and Development Laboratory, Fort Eustis. June 1971.
- [39] P. Crimi. “Prediction of Rotor Wake Flows”. *CAL/U.S.Army Aviation Materiel Laboratories Symposium Proceedings*. Vol. 1. June 1966.
- [40] W. G. Brady and P. Crimi. *Representation of Propeller Wakes by Systems of Finite Core Vortices*. Cornell-Aeronautical Lab. Report No. BB-1655-5-2. February 1965.
- [41] A. R. Trenka. *Development of a Method for Predicting the Performance and Stresses of VTOL-Type Propellers*. U.S.Army Aviation Materiel Laboratories. June 1966.
- [42] J. G. Leishman and M. J. B. A. Bagai. Free Vortex Filament Methods for The Analysis of Helicopter Rotor Wakes. *Journal of Aircraft* **39** (2002).
- [43] S. G. Sadler. “A Method for Predicting Helicopter Wake Geometry, Wake-Induced Flow and Wake Effects on Blade Airloads”. *27th Annual National V/STOL Forum of the American Helicopter Society*. 1972.
- [44] F. N. Coton and T. Wang. The Prediction of Horizontal Axis Wind Turbine Performance in Yawed Flow using an Unsteady Prescribed Wake Model. *Journal of Power and Energy* **213** (1999), pp. 33–43.
- [45] H. Dumitrescu and V. Cardos. Wind Turbine Aerodynamic Performance by Lifting Line Method. *International Journal of Rotating Machinery* **4(1)** (1999), pp. 141–149.
- [46] D. Kocurek. Lifting Surface Performance Analysis for Horizontal Axis Wind Turbines. *SER/STR-217-3163* (1987).
- [47] H. D. Curin, F. N. Coton, and B. Wood. Dynamic Prescribed Vortex Wake Model for AERODYN/FAST. *Journal of Solar Energy Engineering* **130** (2008).
- [48] J. C. Gohard. *Free Wake Analysis of Wing Turbine Aerodynamics*. ASRL TR-184-14, Aero, Struc. Research Lab., Dept. of Aeronautics, and Astronautics, MIT. 1978.
- [49] J. N. Sørensen and W. Shen. Numerical Modeling of Wind Turbine Wakes. *Journal of Fluids Engineering* **124** (2002), pp. 393–399.
- [50] J. N. Sørensen. Aerodynamic aspects of wind energy conversion. *Annual Review of Fluid Mechanics* **43** (2011), pp. 427–448.
- [51] R. Mikkelsen. *Actuator Disc Methods Applied to Wind Turbines*. PhD dissertation, Department of Mechanical Engineering, DTU, Lyngby, 2003.
- [52] N. Troldborg. *Actuator Line Modeling of Wind Turbine Wakes*. PhD thesis, Fluid Mechanics, Department of Mechanical Engineering, Technical University of Denmark, June 2008.
- [53] B. Sanderse, S. P. van der Pijl, and B. Koren. Review of computational fluid dynamics for wind turbine wake aerodynamics. *Journal of Wind Energy* **14(7)** (2011), pp. 799–819.

- [54] M. O. L. Hansen, J. N. Sørensen, J. A. Michelsen, and N. N. Sørensen. “A Global Navier-Stokes Rotor Prediction Model”. *35th Aerospace Sciences Meeting and Exhibit Reno, NV, USA*. 1997.
- [55] H. A. Madsen. “A CFD Analysis for the Actuator Disc Flow Compared with Momentum Theory Results”. *Proceedings of the 10th IEA symposium on the aerodynamics of wind turbines*. The Technical University of Denmark, 1996, pp. 109–124.
- [56] M. E. Berkman, L. N. Sankar, C. R. Berezin, and M. S. Torok. A Navier-Stokes/Full-Potential/Free Wake Method for Rotor Flows. *AIAA Paper 97-0401* ().
- [57] G. Xu and L. N. Sankar. *Journal of Solar Energy Engineering*. **122(1)** (2000), pp. 35–39.
- [58] S. Schmitz and J. J. Chattot. A Coupled Navier-Stokes/Vortex-Panel Solver for the Numerical Analysis of Wind Turbines. *Computers and Fluids* **35** (2006), pp. 742–745.
- [59] P. G. Saffman. *Vortex Dynamics*. Cambridge University Press, Cambridge, UK, 1992.
- [60] D. R. Clark and A. C. Leiper. The Free Wake Analysis - A Method for the Prediction of Helicopter Rotor Hovering Performance. *Journal of the American Helicopter Society* **15(1)** (1970), pp. 3–11.
- [61] T. A. Egolf and A. J. Landgrebe. *A Prescribed Wake Rotor Inflow and Flow Field Prediction Analysis*. User’s Manual and Technical Approach. NASA CR-165894, Langley Research Center, Hampton, VA, 1982.
- [62] W. Johnson. Airloads and Wake Models for a Comprehensive Helicopter Analysis. *Vertica* **14(3)** (1990), pp. 255–300.
- [63] A. J. Landgrebe. An Analytical Method for Predicting Rotor Wake Geometry. *Journal of the American Helicopter Society* **14(4)** (1969), pp. 20–32.
- [64] A. Leonard. “Numerical simulation of interacting three dimensional vortex filaments”. *Proceedings of the Fourth International Conference on Numerical Methods in Fluid Dynamics*. Vol. 35 of series Lecture Notes in Physics. Springer Berlin Heidelberg, 1975, pp. 245–250.
- [65] H. A. Saberi and M. D. Maisel. “A Free-Wake Rotor Analysis Including Ground Effect”. *43rd Annual Forum of the American Helicopter Society, St Louis, MO*. 1987, pp. 879–889.
- [66] S. G. Sadler. *Main Rotor Free Wake Geometry Effects on Blade Air Loads and Response for Helicopters in Steady Maneuvers-Theoretical Formulation and Analysis of Results, Volume I*. User’s Manual and Technical Approach. NASA CR-2110, Langley Research Center, Langley, VA, 1972.
- [67] W. Van Hoydonck. *Computation of Rotorcraft Wake Geometry using NURBS*. PhD thesis, Delft University of Technology, Netherlands, 2013.
- [68] D. B. Bliss, M. E. Teske, and T. R. Quackenbush. *A New Methodology for Free Wake Analysis Using Curved Vortex Elements*. Tech. rep. NASA CR-3958, Ames Research Center, 1987.
- [69] A. Leonard. Vortex Methods for Flow Simulation. *Journal of Computational Physics* **37(3)** (1980), pp. 289–335.
- [70] G. H. Cottet and P. Koumoutsakos. *Vortex Methods: Theory and Practice*. Cambridge University Press, Cambridge, 2000.

- [71] J. D. Anderson. *Fundamentals of Aerodynamics*. 3rd edition. McGraw-Hill, 2001.
- [72] O. M. Knio and A. F. Ghoniem. Numerical study of a three-dimensional vortex method. *Journal of Computational Physics* **86(1)** (1990), pp. 75–106.
- [73] G. Batchelor. *An Introduction to Fluid Dynamics*. Cambridge University Press, Cambridge, UK, 1967.
- [74] J. Katz and A. Plotkin. *Low-Speed Aerodynamics*. 2nd edition. Cambridge University Press, 2001.
- [75] W. Johnson. *Helicopter Theory*. Princeton University Press, Princeton, New Jersey, 1980.
- [76] K. Karamcheti. *Principles of Ideal-Fluid Aerodynamics*. 2nd edition. Florida USA: Krieger, 1980.
- [77] A. Leonard. Computing Three-Dimensional Incompressible Flows with Vortex Elements. *Annual Review of Fluid Mechanics* **17** (1985), pp. 523–559.
- [78] A. V. Garrel. *Requirements for a Wind Turbine Aerodynamics Simulation Module*. 1st edition. ECN report, ECN-C-01-099. 2001.
- [79] M. P. Scully. *Computation of helicopter rotor wake geometry and its influence on rotor harmonic airloads*. PhD thesis, Massachusetts Institute of Technology, Massachusetts, MA, 1975.
- [80] L. Rosenhead. “The Spread of Vorticity in the Wake Behind a Cylinder”. *Proceedings of the Royal Society of London. Series A, Mathematical and Physical Sciences*. Vol. 127(806). 1930, pp. 590–612.
- [81] G. S. Winckelmans. *Topics in Vortex Methods for the Computation of Three and Two-Dimensional Incompressible Unsteady Flows*. PhD thesis, California Institute of Technology, Pasadena, CA, 1989.
- [82] D. B. Bliss. *The Dynamics of Curved Rotational Vortex Lines*. MSc thesis, Massachusetts Institute of Technology, Cambridge, Massachusetts, 1970.
- [83] J. G. Leishman. *Principles of Helicopter Aerodynamics*. 2nd edition. Cambridge Aerospace Series. Cambridge University Press, Cambridge, 2006.
- [84] M. J. Bhagwat and J. G. Leishman. “Generalized Viscous Vortex Model for Application to Free-Vortex Wake and Aeroacoustic Calculations”. *58th Annual Forum and Technology Display of the American Helicopter Society International*. Montreal, Canada, Nov. 2002.
- [85] M. Ramasamy and J. G. Leishman. A Reynolds Number Based Blade Tip Vortex Model. *Journal of the American Helicopter Society* **52(3)** (2007), pp. 214–223.
- [86] M. Bhagwat and G. J. Leishman. Correlation of Helicopter Rotor Tip Vortex Measurements. *AIAA Journal* **38(2)** (2000), pp. 301–308.
- [87] W. J. M. Rankine. *Manual of Applied Mechanics*. Griffen Co., London, 1858.
- [88] M. P. Scully and J. P. Sullivan. *Helicopter Rotor Wake Geometry and Airloads and Development of Laser Doppler Velocimeter for Use in Helicopter Rotor Wakes*. Technical Report 183, MIT DSR No. 73032. Massachusetts Institute of Technology Aerophysics Laboratory, Aug. 1972.
- [89] G. H. Vassitas, V. Kozel, and W. C. Mih. A Simpler Model for Concentrated Vortices. *Experiments in Fluids* **11(1)** (1991), pp. 73–76.
- [90] A. Bagai and J. G. Leishman. Flow Visualization of Compressible Vortex Structures using Density Gradient Techniques. *Experiments in Fluids* **15** (1993), pp. 431–442.

- [91] A. Bagai. *Contribution to the Mathematical Modeling of Rotor Flow-Fields using a Pseudo-Implicit Free Wake Analysis*. University of Maryland, Department of Aerospace Engineering, 1995.
- [92] H. Abedi. *Development of Vortex Filament Method for Aerodynamic Loads on Rotor Blades*. Licentiate thesis, Department of Applied Mechanics, Chalmers University of Technology, Göteborg, 2013.
- [93] S. Gupta and J. G. Leishman. “Stability of Methods in The Free-Vortex Wake Analysis of Wind Turbines”. *23rd ASME Wind Energy Symposium and the 42nd AIAA Aerospace Science Meeting*. Reno NV, May 2004.
- [94] W. Bierbooms. A Comparison between Unsteady Aerodynamic Models. *Journal of Wind Engineering and Industrial Aerodynamics* **39** (1992), pp. 23–33.
- [95] T. S. R. Reddy and K. R. V. Kaza. *Analysis of an Unswept Propfan Blade With a Semi empirical Dynamic Stall Model*. NASA Technical Memorandum 4083. January 1989.

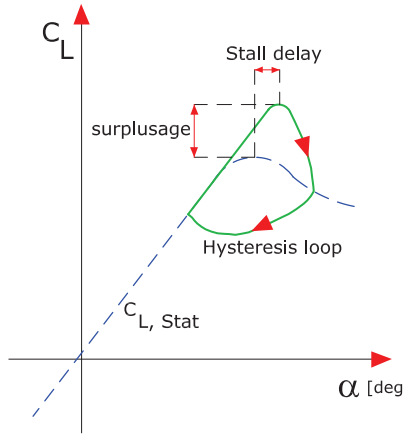


Figure A.1: *Hysteresis loop around the stall angle*

A Extended ONERA Model

In steady flow, when the angle of attack for some blade regions exceeds from the critical angle of attack (α_{stall}), which is equivalent to the maximum lift coefficient ($C_{L,max}$), the flow is separated. This phenomenon is called static stall. This phenomenon, for an airfoil in an unsteady flow, is associated with so-called dynamic stall where its major effect is stall delay and an excessive force (see Fig. A.1). In other words, when an airfoil or a lifting surface is exposed to time-varying pitching, plunging and incident velocity, the stall condition happens at an angle of attack higher than the static stall angle which means that the flow separates at a higher angle of attack than in steady flow. When stall occurs there is a sudden decrease in lift. By decreasing the angle of attack, the flow re-attaches again (stall recovery), but at a lower angle than the static stall angle [95]. This scenario, which is called dynamic stall, occurs around the stall angle and the result is hysteresis loops and a sudden decrease of the lift coefficient. Hence, the dynamic stall describes a series of event resulting in dynamic delay of stall to angles above the static stall angle and it provides the unsteady evolution of lift, drag and moment coefficients along the rotor blade.

In Eqs. (3.21) and (3.22), S_L , K_L and σ_D are airfoil dependent coefficients. However, in case of no wind tunnel measurement data, the flat plate values are applied as $S_L = \pi$ and $K_L = \pi/2$ for small Mach number. The term σ_D is expressed by

$$\sigma_D = \sigma_{0D}\alpha + \sigma_{1D} | \Delta C_L | \quad (\text{A.1})$$

where for the flat plate, $\sigma_{0D} = 0$ and $\sigma_{1D} = 0$. Moreover, $\Delta C_L = C_{L,Lin} - C_{L,Stat}$ where the *Lin* and *Stat* subscripts represent the linear region and the static condition, respectively (see Figs. A.2 and A.3). The linear circulation concerning the attached flow

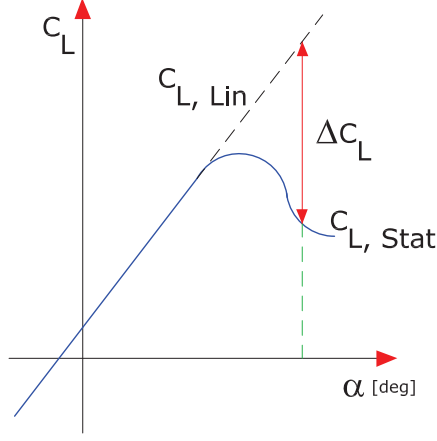


Figure A.2: Definition of the lift coefficient parameters in the ONERA model

lift (Γ_{1L}) is calculated by the first-order differential equation as

$$\begin{aligned} \dot{\Gamma}_{1L} + \lambda_L \frac{2V_p}{c} \Gamma_{1L} = & \lambda_L \frac{2V_p}{c} \left(\frac{dC_L}{d\alpha} \right)_{Lin} (W_0 - V_p \alpha_0) + \lambda_L \frac{2V_p}{c} \sigma_L W_1 \\ & + \left(\alpha_L \left(\frac{dC_L}{d\alpha} \right)_{Lin} + d_L \right) \dot{W}_0 + \alpha_L \sigma_L \dot{W}_1 \end{aligned} \quad (\text{A.2})$$

where V_p , $dC_L/d\alpha$ and α_0 are the total velocity component parallel to the airfoil chord, slope of the C_L vs. α curve in the linear region and the zero-lift angle of attack of each blade element, respectively.

The non-linear circulation concerning the stall correction of lift (Γ_{2L}) is calculated by the second-order differential equation as

$$\ddot{\Gamma}_{2L} + a_L \frac{2V_p}{c} \dot{\Gamma}_{2L} + r_L \left(\frac{2V_p}{c} \right)^2 \Gamma_{2L} = -r_L \left(\frac{2V_p}{c} \right)^2 V_p \Delta C_L - e_L \frac{2V_p}{c} \dot{W}_0 \quad (\text{A.3})$$

Furthermore, the non-linear circulation concerning the stall correction of drag (Γ_{2D}) is given by the second-order differential equation as

$$\ddot{\Gamma}_{2D} + a_D \frac{2V}{c} \dot{\Gamma}_{2D} + r_D \left(\frac{2V}{c} \right)^2 \Gamma_{2D} = -r_D \left(\frac{2V}{c} \right)^2 V \Delta C_D - e_D \frac{2V}{c} \dot{W}_0 \quad (\text{A.4})$$

In Eqs. (3.21), (A.2), (A.3) and (A.4), the symbol $(\dot{\quad})$ denotes the derivation with respect to time.

In the above equations, λ_L , σ_L and α_L depend on the specific airfoil type and they must be determined from experimental measurements. If experimental data for a particular airfoil are not available, these coefficients take the flat plate values as $\lambda_L = 0.17$, $\sigma_L = 2\pi$,

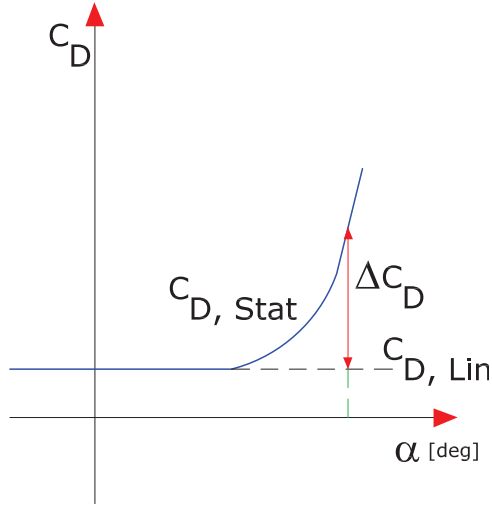


Figure A.3: Definition of the drag coefficient parameters in the ONERA model

$\alpha_L = 0.53$. d_L in Eq. (A.2) and the coefficients in Eqs. (A.3) and (A.4) are functions of ΔC_L due to the flow separation and they are defined as

$$\begin{aligned}
 d_L &= \sigma_{1L} | \Delta C_L | \\
 a_L &= a_{0L} + a_{2L} (\Delta C_L)^2 \\
 a_D &= a_{0D} + a_{2D} (\Delta C_L)^2 \\
 \sqrt{r_L} &= r_{0L} + r_{2L} (\Delta C_L)^2 \\
 \sqrt{r_D} &= r_{0D} + r_{2D} (\Delta C_L)^2 \\
 e_L &= e_{2L} (\Delta C_L)^2 \\
 e_D &= e_{2D} (\Delta C_L)^2
 \end{aligned} \tag{A.5}$$

The coefficients in Eq. (A.5) are airfoil dependent. In case of no wind tunnel measurements, the values for a mean airfoil may be taken and the flat plate values cannot be used. For the mean airfoil, $\sigma_{1L} = 0.0$, $a_{0L} = 0.1$, $a_{2L} = 0.0$, $r_{0L} = 0.1$, $r_{2L} = 0.0$, $e_{2L} = 0.0$, $a_{0D} = 0.0$, $a_{2D} = 0.0$, $r_{0D} = 0.1$, $r_{2D} = 0.0$ and $e_{2D} = 0.0$.

